Differentiation History of the Mesosiderite Parent Body: Constraints from Trace Elements and Manganese-Chromium Isotope Systematics in Vaca Muerta Silicate Clasts

M. WADHWA[1], A. SHUKOLYUKOV[2], A.M. DAVIS[3], G.W. LUGMAIR[2,4] AND D. W. MITTLEFEHLDT[5]

[1]Department of Geology, The Field Museum, 1400 S. Lake Shore Dr., Chicago, IL 60605, USA

[2]Scripps Institution of Oceanography, University of California at San Diego, La Jolla, CA 92093, USA

[3]Enrico Fermi Institute and Department of the Geophysical Sciences, University of Chicago, Chicago, IL 60637, USA

[4]Max-Planck-Institute for Chemistry, Cosmochemistry, PO 3060, 55020 Mainz, Germany

[5]NASA Johnson Space Center, Mail Code SR, Houston, TX 77058, USA

Submitted to

Geochimica Cosmochimica Acta

February 2003

Abstract−We report here the results of a study of trace element microdistributions and ^{53}Mn-^{53}Cr systematics in several basaltic and orthopyroxenitic clasts from the Vaca Muerta mesosiderite. Ion microprobe analyses of selected trace and minor element abundances in minerals of the silicate clasts indicate that, following igneous crystallization, these clasts underwent extensive metamorphic equilibration that resulted in intra- and inter-grain redistribution of elements. There is also evidence in the elemental microdistributions that these clasts were subsequently affected to varying degrees by alteration resulting from redox reactions involving the indigenous silicates and externally derived reducing agents (such as phosphorous, derived from the mesosiderite metal) at the time of metal-silicate mixing. Furthermore, our results suggest that the varying degrees of alteration by redox reactions recorded in the different clasts were most likely facilitated by different degrees of remelting induced by heating during the metal-silicate mixing event. After taking into account the effects of these post-magmatic secondary processes, comparison of the trace and minor element concentrations and distributions in minerals of basaltic and orthopyroxenitic clasts with those of noncumulate eucrites and diogenites, respectively, suggests that the primary igneous petrogenesis, including parent magma and source compositions, of Vaca Muerta silicates were similar to those of achondritic meteorites of the Howardite-Eucrite-Diogenite (HED) association. Internal ^{53}Mn-^{53}Cr isochrons obtained for two basaltic (pebble 16 and 4679) and two orthopyroxenitic (4659 and 4670) clasts show that chromium isotopes are completely equilibrated within each clast. Nevertheless, just as for noncumulate eucrites and diogenites, ^{53}Cr excesses in bulk samples of the basaltic clasts (~1.01 ε in pebble 16; ~1.07 ε in 4679) are significantly higher than in the orthopyroxene-rich clasts (~0.62 ε in 4659; ~0.53 ε in 4670). As also in the case of the HED parent body, this suggests that Mn/Cr fractionation in the parent body of the Vaca Muerta silicate clasts occurred very early

in the history of the solar system, when ^{53}Mn was still extant. However, the slope of the ^{53}Mn-^{53}Cr isochron defined by the whole-rocks of Vaca Muerta clasts (corresponding to a ^{53}Mn/^{55}Mn ratio of $3.3 \pm 0.6 \times 10^{-6}$) is distinctly lower than that defined by the HED whole-rocks (corresponding to a ^{53}Mn/^{55}Mn ratio of $4.7 \pm 0.5 \times 10^{-6}$), indicating that the global Mn/Cr fractionation event that established mantle source reservoirs on the parent body of the Vaca Muerta silicate clasts occurred ~2 Ma after a similar event on the HED parent body.

1. INTRODUCTION

Mesosiderites are stony-iron meteorites that are composed of almost equal proportions of silicates and Fe-Ni metal. While the silicates in these meteorites are comprised of brecciated mixtures of mostly basaltic, gabbroic and pyroxenitic lithologies (Prior, 1918; Powell, 1971; Floran, 1978; Mittlefehldt, 1979), the original bulk composition of the metal that mixed with these silicates is most comparable to that of the IIIAB irons that are thought to have originated in the core of an asteroidal body (Wasson et al., 1974; Hassanzadeh et al., 1990). Therefore, these meteorites represent mixtures of mainly crustal and core materials of differentiated asteroidal bodies and contain only very minor amounts, if any, of the olivine-rich mantle material. Although numerous mechanisms have so far been proposed for producing these silicate-metal mixtures (Hewins, 1983 and references therein; Wasson and Rubin, 1985; Hassanzadeh et al., 1990; Scott et al., 2001), the formation history of mesosiderites and the origin of their components remain rather enigmatic.

In this work, we focus on the question of the origin of silicate clasts in mesosiderites and the implications for the differentiation history of the mesosiderite parent body (MPB). Previous studies of mesosiderite silicates have focused primarily on their petrologic and bulk geochemical characteristics (McCall, 1966; Powell, 1971; Floran, 1978; Mittlefehldt, 1979, 1990; Nehru et al., 1980; Delaney et al., 1980, 1981; Rubin and Jerde, 1987, 1988; Ikeda et al., 1990; Kimura et al., 1991; Rubin and Mittlefehldt, 1992). These investigations have shown that although there are broad similarities in the petrographic and geochemical characteristics of mesosiderite silicates with those of the achondritic meteorites of the Howardite-Eucrite-Diogenite (HED) association, there are also systematic differences that make it improbable for these materials to

have originated on the same parent body. There has been limited work done so far on characterizing the distributions of trace elements that are diagnostic indicators of igneous petrogenesis and post-magmatic processes, such as the rare earth elements, within minerals in these silicates (Crozaz et al., 1985; Kennedy et al., 1992; Mittlefehldt et al., 1992).

A major complicating factor in deciphering the origin and petrogenesis of the mesosiderite silicates is that they have undergone multiple episodes of secondary thermal processing (most likely including metamorphic equilibration and redox reactions) that have affected their petrologic and geochemical characteristics to varying degrees. Therefore, it has been difficult to unravel the effects of post-magmatic processes from the primary magmatic signatures in the mesosiderite silicates. Powell (1971) classified mesosiderites into three sub-groups on the basis of the degree to which their silicates had been recrystallized and metamorphosed (sub-groups I-III; silicates in sub-group I are the least affected and in sub-group III are the most affected). We have chosen to study silicate clasts from a sub-group I mesosiderite, Vaca Muerta (hereafter referred to as VM), to avoid clasts with the highest degrees of secondary thermal processing. Nevertheless, even within a sub-group I mesosiderite such as VM, the degree of alteration resulting from post-magmatic thermal processing of the silicate clasts can be quite variable from clast to clast. Additionally, within VM, there are a variety of clast types, some of which formed by remelting of mixed sources ("polygenic") while others formed from single lithologic sources ("monogenic", which include basalts and gabbros formed from primary melts on the MPB and those formed from remelting of a single lithology) (Rubin and Mittlefehldt, 1992). Since our aim was to infer the differentiation history of the MPB through constraints on the primary igneous petrogenesis of mesosiderite silicates, we selected for this study several monogenic basaltic and orthopyroxenitic clasts that were thought to have formed from endogenous igneous

processes on the MPB. The specific goals of this work include (i) characterization of the microdistributions of trace and minor elements within minerals in selected VM silicate clasts in order to ascertain the extent to which metamorphic equilibration and/or redox reactions have altered primary igneous signatures (this would, furthermore, be useful in determining the petrogenesis of these clasts and also allow comparison with the HEDs), and (ii) obtaining chronological constraints on the differentiation history and evolution of their parent body through studies of ^{53}Mn-^{53}Cr systematics.

2. EXPERIMENTAL METHODS

2.1. Scanning Electron Microscopy and Secondary Ion Mass Spectrometry

Polished thin sections were obtained for five basaltic clasts (pebble 16, 4671, 4677, 4679 and 4695) and two orthopyroxenitic clasts (4659 and 4670) from the Vaca Muerta (VM) mesosiderite. Backscattered electron images were made of each of these thin sections using the University of Chicago JEOL JEM-5800LV scanning electron microprobe (SEM), equipped with an Oxford/Link ISIS-300 energy dispersive microanalysis system. X-ray mapping of selected elements was performed to locate minor and trace minerals such as phosphates.

Subsequent to the SEM documentation, the abundances of the rare earth elements (REE) and yttrium were measured in situ in selected minerals of the five basaltic clasts (pebble 16, 4671, 4677, 4679 and 4695) and one orthopyroxenitic clast (4659) with the University of Chicago AEI IM-20 secondary ion mass spectrometer. In addition to the rare earth elements (REE) and yttrium (Y), concentrations of other elements (including Mg, Al, Ti, Mn, Fe, Zr, and Hf in the

low-Ca pyroxenes and Na, K, Sr, and Ba in the plagioclases) were also measured in selected minerals in these clasts. Analytical techniques used for the ion microprobe analyses were similar to those described by MacPherson and Davis (1994) and references therein. A mass-filtered 20 kV $^{16}O^-$ primary beam was used and count rates at masses of interest were measured using magnetic peak switching at low mass resolution ($M/\Delta M = 500$). Primary beam current ranged from 10 to 50 nA, and resulted in a spot size 15-50 μm in diameter. Energy filtering was used to minimize the contributions from molecular interferences. Calcium-normalized ion yields and interferences were determined from silicate minerals and NBS glasses.

2.2. Measurement of Mn/Cr ratios and Cr Isotopic Composition

Bulk samples were obtained for two basaltic (pebble 16 and 4679) and two orthopyroxenitic (4659 and 4670) clasts from VM. Mn/Cr ratios and Cr isotopic composition were measured in the silicate, chromite, and whole-rock fractions of each of these four clasts. General procedures, summarized below, are similar to those described in more detail by Lugmair and Shukolyukov (1998).

To ensure that the whole-rocks of the analyzed clasts are representative, we used reasonably large bulk samples (>200 mg) for this work. All washing, dissolution and chemical procedures were performed under clean laboratory conditions. Bulk samples were washed in quartz-distilled water, acetone and methanol under ultrasonication. After washing, the samples were dried and weighed. Subsequently, these samples were crushed in a boron carbide mortar. The crushed samples were treated with an HF/HNO_3 mixture, followed sequentially by HNO_3 and HCl. All silicates were dissolved by this treatment, leaving a residue of chrome-spinel that is resistant to

dissolution in these acids at room pressure-temperature conditions. The dissolved silicates were decanted and the chromite residue was washed 3 times with quartz-distilled water; each of the 3 washes was added to the dissolved silicate solution. The chromite fraction was then dissolved in a HF/HNO_3 mixture at high temperature (180°C) in a Teflon pressure bomb. 10-20% of the dissolved silicate and chromite fractions for each clast were quantitatively recombined to produce whole-rock solutions.

After dissolution and equilibration, small aliquots (≤5%) of the silicate, chromite and whole-rock solutions were taken for measurement of Cr and Mn concentrations. The Cr and Mn concentrations were measured by graphite furnace atomic absorption (AA) spectrometry using standard addition techniques. Fe concentrations were additionally measured by flame AA. Repeat measurements of Cr, Mn and Fe abundances in silicate, chromite and whole-rock aliquots of pebble 16, 4659 and 4670, and in chromite and whole-rock aliquots of 4679 were made with a Perkin Elmer inductively coupled plasma optical emission spectrometer (ICP-OES). From reproducibility and comparison with standard samples, accuracy of concentration measurements is estimated to be ~±5% (except for the 4679 silicate fraction that was only analyzed with the AA, in which case the accuracy is estimated to be ~±10%).

Separation of Cr from aliquots of the silicate, chromite and whole-rock solutions was performed using cation exchange chromatography with procedures similar to those followed by Lugmair and Shukolyukov (1998) and adapted from Birck and Allègre (1988). Isotopic composition of Cr was then measured in the silicate, chromite and whole-rock samples for pebble 16, 4679, 4659 and 4670 with the La Jolla VG-54E single-collector thermal ionization mass spectrometer. Mass spectrometric methods are identical to those described by Lugmair and Shukolyukov (1998). For each sample, 12-35 repeat measurements (each comprised of 300

ratios) of the chromium isotopic composition were performed, and the results were averaged. As described previously (Lugmair and Shukolyukov, 1998), the uncertainty on the average $^{53}Cr/^{52}Cr$ for each sample is based on the reproducibility of the repeat measurements of that sample and ranges from 0.07 to 0.12 ε-units. This estimate of the external precision is more conservative than the $2\sigma_{mean}$ uncertainties on the average $^{53}Cr/^{52}Cr$ for each sample (typically by a factor of ~2).

VM has a long exposure age (133 ± 12 Ma; Begemann et al., 1976) and, therefore, it is necessary to make a correction for ^{53}Cr and ^{54}Cr produced by spallation reactions, especially for Fe-bearing phases with relatively high Mn/Cr ratios (since Fe is the main target for spallogenic Cr production). Based on the concentration of Fe in each sample, we estimated the spallation corrected $^{53}Cr/^{52}Cr$ ratio using a production rate of $\sim 2.9 \times 10^{11}$ atoms/g per Ma for both ^{53}Cr and ^{54}Cr (determined from analysis of the iron meteorite Grant; Birck and Allègre, 1988). The spallogenic Cr component is negligible in the chromite fractions and no correction was necessary for these samples. For the whole-rock samples, the correction for spallogenic Cr resulted in an increase in the corrected $^{53}Cr/^{52}Cr$ ratio of 2-3 ppm in the basaltic clasts and ≤1 ppm in the orthopyroxenitic clasts. The spallation correction is somewhat larger for the silicate fractions, and resulted in an increase in the $^{53}Cr/^{52}Cr$ ratio of 7-8 ppm in the basaltic clasts and 4-6 ppm in the orthopyroxenitic clasts.

3. SAMPLE DESCRIPTIONS

The Vaca Muerta (VM) mesosiderite was found in 1861 in the Atacama desert in Chile. The clasts used in this study had weathered out of the metal matrix before they were collected.

Petrographic descriptions, mineral compositions and whole-rock geochemistry (including bulk REE, siderophile and chalcophile element concentrations) have been reported for these clasts by Kimura et al. (1991) and Rubin and Mittlefehldt (1992), and are included in the descriptions below. The numbering of the clasts is as given by these authors. The following description of the clasts studied here is, therefore, based largely on the previous work noted above but also includes results obtained as part of this work (specifically, the distributions of phosphates, opaques and silica from SEM documentation and molar Fe/Mn ratios and mg#, i.e., atomic [Mg/(Mg + Fe)], in the pigeonites determined from the ion microprobe measurements).

3.1. Basaltic Clasts

3.1.1. Texture and Mineralogy

The basaltic clasts studied here have medium- to fine-grained subophitic textures and are composed predominantly of two pyroxenes (mostly pigeonite and some augite) and plagioclase. The pigeonite is typically fine augite exsolution lamellae (usually a few microns in thickness) parallel to (100) and rare occurrences of thicker augite lamellae parallel to (001). In addition to occurring as lamellae in pigeonite, augite also occurs as small isolated grains. Minor and trace minerals include phosphates, silica and opaques (i.e., chromite, ilmenite, troilite and metal). These clasts have been classified as "monogenic" (and likely resulting from endogenous igneous processes on the MPB) by Rubin and Mittlefehldt (1992) and are described here in order of increasing degree of secondary thermal processing (i.e., pebble 16 and 4671 being the least altered and 4677 being the most altered). The following characteristics were taken as the main

indicators of the extent of secondary thermal alteration (Mittlefehldt, 1979, 1990; Rubin and Mittlefehldt, 1992): (i) modal abundances of silica and merrillite; clasts with low modal abundances of these minerals, similar to those in the noncumulate eucrites (i.e., ≤4% silica and <0.1% merrillite; Delaney et al., 1984a), are least affected while those with more abundant silica and merrillite are correspondingly altered to a greater extent; (ii) molar Fe/Mn ratio in the pigeonites; this ratio is typically ~35-37 in the least altered clasts, but can be significantly lower in highly altered clasts.

Pebble 16 is the most fine-grained (with typical grain sizes ≤200 μm) of the basaltic clasts studied here, although there are clusters of larger-sized pyroxene (≤2000 μm) and plagioclase (≤1000 μm) grains (Fig. 1). It is composed of ~60% (mostly low-Ca) pyroxene, ~36% plagioclase, ~3% silica, minor amounts of various opaques (chromite, ilmenite, troilite and metal), and trace amounts (<0.1%) of phosphates (we noted the presence of merrillite as well as apatite). Pigeonites in this clast have molar Fe/Mn ratios of 36-37 (mg# ~0.35).

4671 has an average grain size (≤500 μm) that is intermediate between that for the fine-grained pebble 16 and the medium-grained clasts 4695 and 4679 (Fig. 2a). It is composed of ~53% pyroxene (~44% pigeonite and ~9% augite), ~41% plagioclase, ~4% silica, minor amounts of opaques, and trace amounts (~0.1%) of phosphates (merrillite and apatite). Pigeonites have molar Fe/Mn ratios of 36-37 (mg# ~0.35-0.36).

4695 is a medium-grained clast (Fig. 2b) composed of ~54% pyroxene (~42% pigeonite and ~12% augite), ~41% plagioclase, ~3% silica, minor amounts of opaques, and trace amounts (~0.1%) of merrillite. Pigeonites have molar Fe/Mn ratios of ~35 (mg# ~0.36-0.37). This clast has a somewhat heterogeneous texture on the mm-scale, somewhat similar to 4679 (see below), although to a lesser degree.

4679 has a heterogeneous texture on the mm-scale (Fig. 2c). It is predominantly medium-grained, containing ~58% pyroxene (~43% pigeonite and ~15% augite), ~39% plagioclase, ~2% silica and minor amounts of opaques and trace amounts of merrillite. However, it contains mm-sized pockets of finer-grained material that are enriched in merrillite, silica, and opaques relative to the rest of the matrix. Pigeonites in these phosphate-rich pockets are typically smaller in size than those in the rest of the matrix and are characterized by molar Fe/Mn ratios as low as ~30 (and mg# ~0.42), whereas this ratio is typically ~34-35 (mg# ~0.37-0.38) in pigeonites in the rest of the matrix. In the rest of the text, the phosphate-rich fine-grained areas in 4679 (and the somewhat similar, but less abundant, areas in 4695) will be referred to as the "P-rich pockets", whereas the rest of the clast will be referred to as the "matrix areas".

4677 has a somewhat brecciated fine- to medium-grained ophitic texture (Fig. 2d). The brecciated areas are generally finer-grained and contain abundant phosphate and opaque phases. Overall, this clast is composed of ~55% pyroxene (~37% pigeonite and ~18% augite), ~27% plagioclase, ~11% silica, ~4% troilite, ~1% chromite, ~1% metal, and minor amounts of ilmenite and merrillite. Of all the clasts studied here, this clast has the most abundant silica, phosphate and opaque phases. Pigeonites in this clast have molar Fe/Mn ratios of ~29-31 (mg# ~0.42).

3.1.2. Bulk Geochemistry

The bulk mg# of these basaltic clasts ranges from ~0.33 in pebble 16 to ~0.48 in clast 4677. Concentrations of siderophile and chalcophile elements in these clasts are highly variable; the lowest abundances are found in pebble 16 (Co ~6 µg/g, Ni ~66 µg/g, Se ~0.4 µg/g, and Au ~3 ng/g) and the highest are in clast 4677 (Co ~131 µg/g, Ni ~3200 µg/g, Se ~11 µg/g, and Au ~31

ng/g). All five basaltic clasts studied here have unfractionated bulk REE patterns, with relatively high REE abundances (La ~10 × CI), similar to the noncumulate eucrites.

3.2. Orthopyroxenitic Clasts

3.2.1. Texture and Mineralogy

The two orthopyroxene-rich clasts studied here (4659 and 4670) are fine- to coarse-grained breccias (Fig. 3). 4659 is a diogenitic clast composed of ~85% orthopyroxene, ~10% troilite, ~3% metal, ~1% chromite and ~1% merrillite. The molar Fe/Mn ratio in orthopyroxenes of 4659 is ~30-32 (mg# ~0.71-0.75). 4670 is an olivine-orthopyroxenitic clast composed of ~63% orthopyroxene, ~24% olivine, ~7% troilite, ~4% metal, ~1.5% chromite, and ~0.5% merrillite. Compared to monomict orthopyroxenitic breccias of the HED association (i.e., diogenites), these two clasts are highly enriched in opaques and merrillite. Plagioclase, augite and silica do not occur in clast 4659; minor to trace amounts of these minerals have been observed in 4670.

3.2.2. Bulk Geochemistry

The mg# for the bulk sample of clast 4659 is ~0.73, and that for 4670 is ~0.75. Siderophile and chalcophile element abundances in 4659 are high (Co ~115 µg/g, Ni ~15700 µg/g, Se ~13 µg/g and Au ~54 ng/g). As expected for samples consisting predominantly of orthopyroxene (a mineral in which the REE are highly incompatible), bulk REE abundances in 4659 are low (La

<0.4 × CI; Eu <0.5 × CI; Yb <1 × CI). Trace element abundances in a bulk sample of 4670 have not been reported.

4. RESULTS

4.1. Trace and Minor Element Abundances in Minerals of Vaca Muerta Clasts

Results of ion microprobe analyses of minerals in five basaltic clasts and one orthopyroxenitic clast (including the number of analyses performed on each mineral) are given in Tables 1-4 and Figs. 4-6. Abundances of the REE and Y (which behaves as an analog for the HREE) are presented here for phosphates (merrillite and, in case of pebble 16 and 4671, apatite), plagioclase, augite and pigeonite in the basaltic clasts, and for merrillite and orthopyroxene in the orthopyroxenitic clast 4659. Concentrations of several additional elements are also reported for selected minerals (specifically, Mg, Al, Ti, Mn, Fe, Zr and Hf abundances in the low-Ca pyroxenes and Na, K, Sr, and Ba abundances in the plagioclases) in these clasts.

4.1.1. Phosphates

In all the clasts studied here, merrillite is the main REE carrier. However, there is a wide range of REE abundances in this mineral not only between clasts but also within some of the clasts (Table 1; Figs. 4 and 5). In the five basaltic clasts, the REE pattern of merrillite is typically LREE-enriched with a negative Eu anomaly (Fig. 4). However, the degree of LREE enrichment and the size of the Eu anomaly are correlated with absolute REE abundances. Merrillites in

pebble 16 (La ~5,600-8,800 × CI) and 4671 (La ~11,200 × CI), which have the highest REE concentrations, are also the most LREE-enriched (CI-normalized La/Yb ~4-7) and have the largest negative Eu anomalies (Eu/Eu* ~ 0.05-0.08, where Eu* is the value interpolated between CI-normalized abundances of Sm and Gd). REE concentrations in merrillites of 4695 and 4679 vary by a factor of ~6-8 (La ~1,100-6,700 × CI and ~700-5,700 × CI, respectively), with the highest values being similar to those in merrillites of pebble 16 and 4671; the lowest values are similar to those in merrillites of 4677 (La ~500-1000 × CI). Correspondingly, the degree of LREE enrichment and the size of the Eu anomaly is also variable in merrillites of 4695 and 4679 (CI-normalized La/Yb ~2-4; Eu/Eu* ~0.06-0.4); merrillites in 4677 have only slight LREE enrichment (CI-normalized La/Yb ~1.1-1.8) and small Eu anomalies (Eu/Eu* ~0.3-0.5). It is notable that merrillites with the lowest REE abundances (as well as the least LREE enrichment and smallest Eu anomalies) in 4679 occur in the P-rich pockets described earlier in section 3.1.

Merrillites in the orthopyroxenitic clast 4659 have the lowest REE abundances (La ~40-60 × CI) of all the merrillites in the clasts studied here (Table 1; Fig. 5). Additionally, their REE pattern is characterized by LREE depletion (CI-normalized La/Yb ~0.7-0.8), and a slightly positive Eu anomaly (Eu/Eu* ~2-3).

Pebble 16 and 4671 are the only clasts studied here that also contain apatite in addition to the merrillite. REE abundances in apatites of pebble 16 (La ~80-230 × CI) and 4671 (La ~100-650 × CI) are typically lower than those in merrillites of these clasts by 1-2 orders of magnitude (Table 1; Fig. 4ab). The REE patterns are LREE-enriched (CI-normalized La/Yb ~1-2 and ~3-4 in pebble 16 and 4671, respectively), and have negative Eu anomalies (Eu/Eu* ~0.06-0.15 and ~0.03-0.17 in pebble 16 and 4671, respectively).

4.1.2. Plagioclase

Plagioclase is present in the five basaltic clasts. This mineral has a LREE-enriched REE pattern (La ~1-10 × CI; CI-normalized La/Nd ~2-4) and a pronounced positive Eu anomaly (Eu/Eu* ~20-40) (Table 2, Fig. 4). The concentrations REE and Y vary considerably (by a factor of up to ~4 within clasts and ~10-20 between clasts) (Table 2; Fig. 6a). Other minor and trace elements besides the REE (and Y) were also measured in plagioclases of basaltic clasts and are reported in Table 2. Abundances of Na, K, Sr, and Ba in plagioclases of all these clasts are remarkably uniform (within and between clasts) and vary at most by a factor of ~1.5 (Table 2; Fig. 6b). No plagioclase was found to be present in the orthopyroxenitic clasts.

4.1.3. Pyroxenes

As discussed in an earlier section, basaltic clasts contain two pyroxenes (augites and pigeonites). Although both minerals are characterized by HREE-enriched patterns, the augites typically have flatter REE patterns (CI-normalized Sm/Yb ~0.4-0.8 versus ~0.1-0.4 in pigeonites) and higher REE concentrations (La ~0.5-10 × CI versus ~0.05-1 × CI in pigeonites) (Table 3; Fig. 4). Augites in the basaltic clasts studied here, with the exception of 4677, have large negative Eu anomalies (Eu/Eu* ~0.05-0.1); in 4677, this mineral has a significantly smaller negative Eu anomaly (Eu/Eu* ~0.6).

Low-Ca pyroxenes in the basaltic clasts usually consist of pigeonites that contain fine exsolution lamellae of augite. The ion microprobe beam used for analyzing pyroxenes typically resulted in beam spots ~30-50 μm in diameter, much larger than the width of the exsolution

lamellae. Therefore, the compositions shown in Table 4 reasonably approximate the compositions of the original unexsolved pigeonite. Absolute REE abundances and sizes of Eu anomalies in this mineral vary not only between clasts but also within clasts. Specifically, pigeonites in pebble 16, 4671, and 4695 have only a modest range of REE abundances (La ~0.1-0.8 × CI in pebble 16, ~0.1-0.3 in 4671 and ~0.06-0.2 in 4695) and large negative Eu anomalies (Eu/Eu* ~0.05-0.1) (Fig. 4abc). In 4679, pigeonites have the largest spread in REE abundances (La ~0.04-0.7 × CI) (Fig. 4d). Typically, those with La abundances >0.1 × CI have large negative Eu anomalies (Eu/Eu* ~0.1) while those with La abundances <0.1 × CI have smaller Eu anomalies (Eu/Eu* ~0.4-1.0) and appear to occur predominantly in the P-rich pockets of 4679. Pigeonites in 4677 have a small range of REE abundances (La ~0.1-0.3 × CI) and small Eu anomalies (negative and positive; Eu/Eu* ~0.7-1.4) (Fig. 4e).

Orthopyroxenes in the diogenitic clast 4659 have low absolute REE abundances (La ~0.02-0.06 × CI) and HREE-enriched REE patterns (Table 4; Fig. 5). The CI-normalized Sm/Yb ratios in orthopyroxenes with the highest REE concentrations are ~0.3-0.5; errors on REE abundances are typically too large to constrain Sm/Yb ratios in those with the lowest concentrations. Eu abundances in all orthopyroxenes in 4659 are extremely low (<<0.2 × CI); it is difficult to estimate the sizes of Eu anomalies due to large uncertainties associated with the absolute Eu concentrations.

Other major, minor and trace elements besides the REE were also measured in pigeonites of the basaltic clasts and the orthopyroxenitic clast 4659 and are reported in Table 4. As can be seen from the data in Table 4, there is considerable variation in the abundances of elements such as Ti, Y, Zr and Hf among pigeonites of the basaltic clasts. In these pigeonites, Ti concentrations generally correlate positively with the concentrations of Y (Fig. 6c), Zr (Fig. 6d)

and Hf. However, in the plot of Y versus Ti abundances (Fig. 6c) pigeonites in 4677 and in the P-rich pockets of 4679 define a trend that is distinct from that defined by pigeonites in the other basaltic clasts, whereas in the plot of Zr versus Ti (Fig. 6d) pigeonites of all the basaltic clasts fall along a single trend. Although it is not plotted, Hf behaves similarly to Zr in pigeonites of these basaltic clasts.

Concentrations of Ti, Y, Zr and Hf also vary significantly in orthopyroxenes of the diogenitic clast 4659 (Table 4). However, it is notable that Ti abundances in these orthopyroxenes appear to be anti-correlated with Y concentrations (Fig. 6e), even though they correlate positively with Zr (Fig. 6f) and Hf concentrations.

4.2. ^{53}Mn-^{53}Cr Systematics in Vaca Muerta Clasts

Results of the measurements of Mn/Cr ratios and Cr isotopic compositions of the whole-rock (TR), chromite (Chr) and silicate (Sil) fractions from two basaltic clasts (pebble 16 and 4679) and two orthopyroxene-rich clasts (4659 and 4670) are reported in Table 5 and Fig. 7.

4.2.1. Basaltic Pebble 16

^{55}Mn/^{52}Cr ratios in pebble 16 vary from ~0.011 (in the chromite fraction, Chr) to ~5.88 (in the silicate fraction, Sil). Although ^{53}Cr/^{52}Cr in the chromite fraction appears to be systematically lower than the silicate fraction by ~9 ppm, within the uncertainties the slope of the best-fit line to the data cannot be distinguished from zero. Therefore, although there may be a hint of live ^{53}Mn

being present at the time of last equilibration of Cr isotopes in this sample, only an upper limit for the $^{53}Mn/^{55}Mn$ ratio (i.e., $<4.1 \times 10^{-7}$) can be presented.

4.2.2. Basaltic Clast 4679

$^{55}Mn/^{52}Cr$ ratios range from ~0.014 (Chr) to ~5.71 (Sil). Despite this range in Mn/Cr ratios, total range in $^{53}Cr/^{52}Cr$ for all three measured fractions is only ~1 ppm with an average of 1.07 ε-units. Therefore, Cr isotopes are thoroughly equilibrated in this sample and a strict upper limit for the $^{53}Mn/^{55}Mn$ ratio of $<2.2 \times 10^{-7}$ is estimated.

4.2.3. Orthopyroxene-rich Clast 4659

The spread in the Mn/Cr ratios in the orthopyroxenitic clasts is smaller than that in the basaltic clasts. In 4659, the $^{55}Mn/^{52}Cr$ ratios vary from ~0.020 (Chr) to ~2.82 (Sil). The $^{53}Cr/^{52}Cr$ ratios are the same within uncertainties in all three measured fractions, with a total range in $^{53}Cr/^{52}Cr$ of ~6 ppm. Since Cr isotopes are completely equilibrated, only an upper limit on the $^{53}Mn/^{55}Mn$ ratio of $<4.7 \times 10^{-7}$ can be determined.

4.2.4. Orthopyroxene-rich Clast 4670

$^{55}Mn/^{52}Cr$ ratios in this clast range from ~0.016 (Chr) to ~1.89 (Sil). Total range in the $^{53}Cr/^{52}Cr$ ratios in the Chr, Sil and TR fractions is ~4 ppm. As in the case of the other clasts analyzed here, there does not appear to be any detectable evidence of live ^{53}Mn at the time of last

equilibration of Cr isotopes and only an upper limit on the $^{53}Mn/^{55}Mn$ ratio of $<6.0 \times 10^{-7}$ is estimated.

5. DISCUSSION

5.1. Comparison of Vaca Muerta Silicate Clasts with HEDs: Deconvolving the Effects of Post-Magmatic Thermal Processing on Trace and Minor Element Microdistributions

In the following we will discuss the microdistributions of trace and minor elements in the minerals in the silicate clasts in the context of similarities and differences with the HEDs. We will show that the similarities are a direct result of similar primary igneous petrogenesis of the silicate clasts and the HEDs, followed by broadly similar post-crystallization histories of extensive subsolidus metamorphism. The differences are then explained as a result of the metal-silicate mixing event, which significantly affected the mesosiderite silicates (subsequent to the subsolidus metamorphism), but clearly did not take place in the case of the HEDs.

Prior to making any interpretations, however, it is important to reiterate here what is known from other mineralogical and geochemical indicators regarding the relative degrees of post-magmatic thermal alteration (specifically, that resulting from redox reactions) in the different clasts studied here. As described previously (section 3), comparison of the modal abundance of phosphates and molar Fe/Mn ratios of low-Ca pyroxenes in these clasts with those in the HEDs indicates that, of the five basaltic clasts studied here, pebble 16 and clast 4671 have been least affected; clasts 4695 and 4679 appear to have been affected heterogeneously on the mm-scale; clast 4677 is the most affected. The orthopyroxenitic clasts considered here also appear to be

severely affected by such thermal alteration/redox reactions. We will show here that this record of the varying degrees of secondary thermal alteration is also evident in the trace and minor element microdistributions in individual minerals in each of these clasts.

5.1.1. Subsolidus Metamorphism

Phosphates (merrillites and apatites) in the least affected clasts, pebble 16 and clast 4671, have REE abundances and patterns that fall within the range of those in noncumulate eucrites. It is noteworthy, however, that none of the phosphates in pebble 16 or 4671 have REE concentrations that are as high as in some noncumulate eucrites (i.e., La up to ~25,000 × CI; Delaney et al., 1984b; Hsu and Crozaz, 1996). In fact, REE abundances and patterns in phosphates of pebble 16 and 4671 (Figs. 4ab) are most similar to those in the most highly equilibrated of these samples (specifically, Ibitira, EET90020 and Y86763) (Fig. 4f), whose phosphates have the lowest REE abundances of all noncumulate eucrites analyzed so far (Hsu and Crozaz, 1996; Floss et al., 2000; Yamaguchi et al., 2001). The relatively low REE concentrations in phosphates of the highly equilibrated noncumulate eucrites have been attributed by previous workers to the fact that these eucrites experienced more severe thermal metamorphism than other noncumulate eucrites, thereby resulting in inter-grain equilibration with the REE-poor silicates (whereas the less equilibrated noncumulate eucrites at most experienced only intra-grain equilibration). Therefore, it is evident that phosphates in the least thermally altered of the clasts studied here are altered by subsolidus metamorphism and inter-grain equilibration to a similar degree as some of the most highly metamorphosed noncumulate eucrites. There is further evidence of inter-grain exchange due to severe metamorphic

equilibration in the trace and minor element distributions in plagioclases of the least altered of the basaltic clasts studied here. Specifically, in a plot of Y (or other HREE) versus La (or other LREE) abundances, the compositions of plagioclases in the basaltic clasts lie to the right of the correlation line defined by most noncumulate eucrites (Fig. 6a). It has been previously noted that plagioclases in the most highly equilibrated noncumulate eucrites also lie to the right of this correlation line (in the field defined by the light gray shaded area in Fig. 6a) due to inter-mineral exchange with the LREE-enriched phosphates during extensive heating associated with the thermal metamorphism (Hsu and Crozaz, 1996; Floss et al., 2000; Yamaguchi et al., 2001). It is then reasonable to assume that a similar process resulted in the variable LREE-enrichment observed in the plagioclases of the VM basaltic clasts.

Finally, trace and minor element compositions of low-Ca pyroxenes of the basaltic clasts also lend credence to the idea that, subsequent to crystallization, these clasts were metamorphosed to a degree similar to the most highly equilibrated noncumulate eucrites. In particular, the abundances of elements such as Ti, Y and Zr in low-Ca pyroxenes of pebble 16 and 4671 (and of the matrix areas of 4679 and 4695) lie towards the higher end of the range of concentrations of these elements in pigeonites of noncumulates eucrites. As can be seen in Figs. 6cd, the highest abundances of these elements are to be found in pigeonites of the most equilibrated of noncumulate eucrites such as Ibitira, EET90020 and Y86763 (which appear to have experienced extensive inter-grain exchange of these elements with late-stage phases such as phosphates and oxides that are rich in these incompatible elements). The fact that concentrations of these elements in pigeonites of pebble 16, 4671, and matrix areas of 4679 and 4695 approach those in the most highly equilibrated noncumulate eucrites (Figs. 6cd) indicates that even the least altered

of VM basaltic clasts have experienced a similar process of inter-grain diffusional exchange resulting from severe subsolidus metamorphism.

5.1.2. Secondary Magmatic Reduction

In the two clasts that appear to be altered heterogeneously, 4695 and 4679, some merrillites have REE abundances similar to those in the least altered clasts (pebble 16 and clast 4671), but others have REE concentrations that are lower by an order of magnitude or more (i.e., La ≤~1000 × CI). In the most altered basaltic clast 4677, phosphates are abundant and have REE concentrations similar to the lowest REE abundances found in the phosphates of 4695 and 4679 (i.e., La ≤~1000 × CI). These REE abundances are lower than those in primary magmatic phosphates of the least metamorphosed noncumulate eucrites (Delaney et al., 1984b; Hsu and Crozaz, 1996) by more than a factor of ~20-30. Finally, the abundant phosphates in the diogenitic clast 4659 have the lowest REE concentrations measured here (La ≤~60 × CI) and relatively flat REE patterns (CI–normalized La/Sm ~1-2). By comparison, primary magmatic phosphates are present only in trace modal abundances in diogenites, but are exceedingly LREE-enriched (La ~65,000 × CI and CI-normalized La/Sm ~10; Mittlefehldt, 1994).

In the case of 4679, there appears to be a clear correlation between the petrogenetic setting of the phosphates and their REE content. Specifically, the abundant phosphates located in the fine-grained P-rich pockets have the lowest REE concentrations; isolated phosphates located within the coarser-grained matrix areas have the highest REE abundances. This suggests that the formation of the low REE-content phosphates may be related to the formation of the fine-grained P-rich pockets. In such a scenario, the process responsible for the formation of the fine-grained

P-rich pockets in 4679 occurred on a lesser scale in 4695 (which appears to have fewer low REE-content phosphates) and was much more pervasive in the basaltic clast 4677 and diogenitic clast 4659 (both of which have abundant phosphates with low REE-content). Pebble 16 and clast 4671 largely escaped such a process. What was this mechanism whereby the low REE-content phosphates were produced? It has been suggested previously that pyroxenes (pigeonites and augites) with low molar Fe/Mn ratios in some basaltic mesosiderite clasts were formed as a result of "magmatic reduction processes" (Mittlefehldt, 1990). Specifically, it was suggested that FeO reduction in the interstitial liquid resulted in the formation of late magmatic augite (by driving the liquid composition into pigeonite + augite liquidus field). This same magmatic reduction process, likely resulting from reaction of reducing agents such as P (and C?) with the melt, may also be responsible for the formation of merrillite. The next question that needs to be addressed then is how such a magmatic reduction process was accomplished. We suggest that the original material from which the basaltic and diogenitic clasts were derived was similar in textural and geochemical characteristics to noncumulate eucrites and diogenites, respectively. During the metal-silicate mixing event which is thought to have occurred ~100-150 Ma subsequent to original crystallization (Stewart et al., 1994), the silicate materials were reheated to different degrees depending on the extent of their exposure to the hot (likely molten) metal. Clasts such as pebble 16 and 4671 were hardly affected since they may have been sufficiently shielded by surrounding silicates, whereas clasts such as 4679 and 4695 experienced greater degree of reheating such that their original mesostasis areas (consisting of late-stage phases that crystallized at lower temperatures than the first-formed magmatic minerals) were preferentially remelted and became the sites at which the magmatic reduction took place resulting in the formation of the fine-grained pockets enriched in phosphates. The basaltic clast 4677 and the

diogenitic clast 4659 are likely to have been more extensively reheated, such that they experienced remelting of not just their mesostasis areas but also their matrix minerals. These secondary melts underwent reduction by the addition of elements such as P derived from the metal. The trace element data reported here suggest that the addition of P was plausibly responsible for the production of the abundant phosphates from these secondary melts, which effectively scavenged the REE. The absolute concentrations of the REE, however, are low in these secondary phosphates (compared to the primary magmatic phosphates) since their higher modal abundance has the net effect of "diluting" the REE. Continued reduction of these secondary melts (with reducing agents in addition to P, such as C; Mittlefehldt, 1990) likely resulted in the co-crystallization of the fine-grained pyroxenes (pigeonites and augites in the basaltic clasts and orthopyroxenes in the diogenitic clasts) with lower Fe/Mn ratios than the primary magmatic pyroxenes. Formation of pyroxenes in equilibrium with phosphates (into which the REE partition preferentially) in these secondary melts is supported by their extremely low REE contents (e.g., pigeonites of 4677 and of the P-rich pockets in 4679 in Fig. 6c, as well as the orthopyroxenes of 4659 in Fig. 6e). The fact that the noncumulate eucrites typically do not contain primary magmatic augite and that the modal abundance of the augite in basaltic clasts (negligible in pebble 16 to ~18% in 4677; see section 3.1.1) correlates with their degree of thermal (redox) alteration further suggests that the augite formed as a result of the secondary magmatic reduction process described above.

Finally, it is notable that the degree of thermal (redox) alteration recorded in the VM silicate clasts correlates with their bulk concentrations of siderophile-chalcophile elements (e.g., Ni ~66 μg/g in pebble 16, ~365 μg/g in 4671, ~1040 μg/g in 4695, ~1180 μg/g in 4679, ~3200 μg/g in 4677, and ~15700 μg/g in 4659) and modal abundances of metal (i.e., trace amounts in pebble

16, 0.1% in 4671, 0.2% in 4695 and 4679, 0.9% in 4677, and 2.5% in 4659) (Kimura et al., 1991; Rubin and Mittlefehldt, 1992). There are two possibilities (or perhaps a combination thereof) that could explain this. The metal may be a byproduct of redox reactions, such as those proposed by Agosto et al. (1980) and Harlow et al. (1982), that took place concurrently with the metal-silicate mixing event. In this case, the siderophile-chalcophile elements as well as the reducing agents such as P (and C?) would be added to these clasts by diffusional transport from metal to the silicates. Such diffusional transport is expected to be more easily accomplished in clasts with greater exposure to the hot (molten) metal and which, therefore, experienced greater degrees of remelting and concomitant magmatic reduction. Alternatively, the metal may represent a physical mixture of remelted portions of the silicate clasts with portions of the metallic body that interacted with these VM silicates during the metal-silicate mixing event. In this case, the metal within these clasts would have been the original (and predominant) carrier of the siderophile-chalcophile elements as well as of elements such as P (and C?) that would produce reduction of the secondary melt. A simplistic calculation of the expected abundances of P and Ni in these clasts may be performed assuming that all the P and siderophile-chalcophile elements in the clasts originally resided in the metal now present in these clasts. Further assuming that the admixed metal had bulk contents of P and Ni similar to the average abundances of these elements in IIIAB irons (Hassanzadeh et al., 1990; Buchwald, 1975) and given the modal metal abundances (Kimura et al., 1991; Rubin and Mittlefehldt, 1992), we find that the actual abundances of P and Ni in the most altered clasts (i.e., 4677 and 4659) are higher (by a factor of >15 for P and >3 for Ni) than would be predicted by these calculations. This suggests that although some portion of P and siderophile-chalcophile elements may have been added to the most altered clasts as a result of admixed metal originating from the metallic

impactor, the rest were likely transported through diffusion from surrounding metal into the clasts. It is important to note, however, that in either of the above cases the observed correlation between the modal abundances of metal, concentrations of siderophile-chalcophile elements and the degree of thermal (redox) alteration implies a linkage between the metal-silicate mixing event and secondary magmatic reduction process affecting the VM silicates.

5.1.3. Inferences Regarding Igneous Petrogenesis, Parent Magma and Source Compositions

Although, as shown in the above two sections, the VM silicate clasts studied here have undergone extensive subsolidus metamorphism superimposed by varying degrees of redox reactions (most likely facilitated by varying degrees of remelting during the metal-silicate mixing event), it is still possible to make reasonable inferences regarding their primary igneous petrogenesis from the trace and minor element microdistributions in their minerals.

It is notable here that in plots of concentrations of refractory trace elements (such as Sr and Ba) versus volatile alkali elements (such as Na and K), plagioclase compositions in the basaltic clasts lie on an extension of the trend defined by plagioclase compositions in Ibitira (which in turn lie to the left of the main trend defined by those in other noncumulate eucrites) (Fig. 6b). This alkali element depletion in Ibitira plagioclases has been attributed to one of three possibilities (Stolper, 1977): alkali loss during thermal metamorphism, derivation of the Ibitira parent magma from an alkali-depleted source, or alkali loss during eruption. It has been shown recently that noncumulate eucrites (such as EET90020 and Y86763) that have undergone severe thermal metamorphism to a similar degree as Ibitira do not show the alkali element depletion in their plagioclase compositions (Floss et al., 2000; Yamaguchi et al., 2001). Therefore, it appears

that the alkali depletion in plagioclases of Ibitira as well as in plagioclases of the VM basaltic clasts cannot be attributed to thermal metamorphism, but may either be a primary signature of alkali depletion in their mantle sources or could have resulted from alkali loss from their parent magmas between magma genesis and crystallization. Either one of these two possibilities specifically points to a similarity in the primary petrogenetic history of Ibitira on the one hand and the VM basaltic clasts on the other.

Compositions of low-Ca pyroxenes in the basaltic clasts that are least affected by redox reactions (i.e., pebble 16, 4671, 4695 and the matrix areas of 4679) all lie within the range of compositions defined by pigeonites of noncumulate eucrites (Fig. 6cd). It is notable, however, that most of these compositions appear to the bridge the compositional gap between the most highly equilibrated eucrites on the one hand and the rest of the noncumulate eucrites on the other (Fig. 6cd). Previous studies have suggested that the compositional difference between pigeonites of the most equilibrated eucrites and those of other noncumulate eucrites arise from the fact that pigeonites of the former experienced inter-grain equilibration with late stage phases, whereas pigeonites of the latter only underwent intra-grain equilibration. The data reported here for the low-Ca pyroxenes in the basaltic eucrites then suggests that these pyroxenes experienced intra- as well as inter-grain equilibration during subsolidus metamorphism (the extent of which was similar to or slightly less severe than that suffered by the most equilibrated of the noncumulate eucrites), and that their original (i.e., magmatic, prior to equilibration) trace and minor element compositions were similar to primary magmatic pigeonites of the noncumulate eucrites.

As discussed in the previous section, the extremely low REE and Y abundances in the low-Ca pyroxenes of those basaltic clasts that have been most affected by thermal alteration (4677 and P-rich pockets of 4679) can be attributed to redox reactions and the preferential uptake of these

elements in the secondary phosphates produced during this process. Most of the low-Ca pyroxenes analyzed by us in the orthopyroxenitic clast 4659 also show this extreme depletion of the REE and Y concentrations and this is also attributable to the same process as indicated above. However, some orthopyroxene compositions do overlap those of orthopyroxenes in diogenites (Fig. 6ef). This further suggests that the original magmatic pyroxene compositions in the VM basaltic and orthopyroxenitic clasts are likely to have been similar prior to being altered by varying degrees of subsolidus metamorphism and redox reactions. A necessary corollary to this is that the original magma compositions from which minerals in the VM basaltic and orthopyroxenitic clasts crystallized (and corresponding source regions in the mantle of the VM silicate PB) were similar to the parent magmas (and mantle sources) of the noncumulate eucrites and diogenites, respectively.

5.2. Differentiation History of the Asteroidal Parent Body of the Vaca Muerta Mesosiderite: Clues from Mn-Cr Isotope Systematics

Cr isotopes in the two basaltic clasts, pebble 16 and 4679, and the two orthopyroxenitic clasts, 4659 and 4670, appear to be completely equilibrated, indicating that there was no detectable evidence for live ^{53}Mn present in these clasts at the time of last closure of the Mn-Cr system. This situation is analogous to that in noncumulate eucrites such as Caldera and diogenites such as Shalka and Johnstown (Lugmair and Shukolyukov, 1998) which also show thorough equilibration of Cr isotopes either due to slow cooling or secondary reheating. In the case of the VM silicate clasts, it is plausible that Cr isotopic equilibration occurred during one of the two major secondary thermal episodes experienced by them, i.e., either during the phase of extensive

subsolidus metamorphism or during later reheating at the time of the metal-silicate mixing. In either case, the upper limits estimated on the $^{53}Mn/^{55}Mn$ ratio in each of the clasts studied here (Fig. 7) suggest that this equilibration event must have occurred >20 Ma after solar system formation (or time of incorporation of live ^{53}Mn into the early solar system). We have shown earlier that the extent of subsolidus metamorphism of the VM basaltic clasts was similar to (or slightly less than) that experienced by the highly equilibrated noncumulate eucrite Ibitira, which in fact still retains evidence for the presence of live ^{53}Mn at the time of its last equilibration (Lugmair and Shukolyukov, 1998). This may suggest that the event that resulted in equilibration of Cr isotopes may be the reheating associated with the metal-silicate mixing event (which occurred 100-150 Ma after the beginning of the solar system formation; Stewart et al., 1994).

The significance of the Cr isotopic systematics of the VM silicate clasts in terms of placing constraints on the differentiation history of their parent body lies in the fact that, just as for noncumulate eucrites and diogenites, the ^{53}Cr excesses in bulk samples of the basaltic clasts (~1.01 ε in pebble 16; ~1.07 ε in 4679) are higher than those in bulk samples of the orthopyroxene-rich clasts (~0.62 ε in 4659; ~0.53 ε in 4670). As in the case of the HED parent body, this indicates that Mn/Cr fractionation in the source region of the VM silicate clasts occurred early in the history of the solar system, when ^{53}Mn was still extant. As shown in Fig. 8, the excesses in ^{53}Cr in the bulk samples of the VM silicate clasts are correlated with Mn/Cr ratios and indicate a $^{53}Mn/^{55}Mn$ ratio of $(3.3 \pm 0.6) \times 10^{-6}$ and an initial $^{53}Cr/^{52}Cr$ ratio of 0.41 ± 0.08 ε-units. This correlation is indicative of the fact that the source reservoirs (characterized by different Mn/Cr ratios) of each of these clasts were established contemporaneously and that the Mn-Cr system in the bulk samples have remained closed since their original crystallization. This is broadly similar to Mn-Cr systematics in the HED bulk samples, except for the fact that the

HED "bulk isochron" is characterized by a higher $^{53}Mn/^{55}Mn$ ratio of $(4.7 \pm 0.5) \times 10^{-6}$ and lower initial $^{53}Cr/^{52}Cr$ ratio of 0.25 ± 0.07 ε-units (Lugmair and Shukolyukov, 1998) (Fig. 8).

It has been previously demonstrated, based on Mn-Cr systematics in various meteorite classes believed to have originated within the asteroid belt, that the ^{53}Mn distribution in this region was uniform and that relative differences in $^{53}Mn/^{55}Mn$ ratios may be used to define relative formation ages for such objects (Lugmair and Shukolyukov, 1998, 2001). Furthermore, the ^{53}Mn-^{53}Cr relative chronometer can be tied to an absolute time scale using the angrites Angra dos Reis and LEW86010, which have a precisely determined Pb-Pb age of 4557.8 ± 0.5 Ma (Lugmair and Galer, 1992) with a corresponding $^{53}Mn/^{55}Mn$ ratio of 1.25 ± 0.07 (Lugmair and Shukolyukov, 1998). Given the above, Lugmair and Shukolyukov (1998) determined that the $^{53}Mn/^{55}Mn$ ratio of $(4.7 \pm 0.5) \times 10^{-6}$ defined by bulk samples of eucrites and diogenites corresponded to an absolute age of 4564.8 ± 0.9 Ma. These authors interpreted this age as the time of global Mn/Cr fractionation in the mantle of the HED parent body (PB). Additionally, the fact that the HED bulk isochron passes only marginally above the chondritic point (solid square in Fig. 8 corresponding to a $^{53}Cr/^{52}Cr$ ratio of ~0.48 ε-units at a $^{55}Mn/^{52}Cr$ ratio of 0.76) was taken to be indicative of a chondritic composition for the bulk HED PB.

As indicated earlier, Mn-Cr systematics in the bulk samples of the VM silicate clasts are analogous to those in HED bulk samples, although the slope and initial of the VM silicate isochron is distinctly different from those of the HED isochron (Fig. 8). An additional feature to note regarding the VM isochron is that it passes farther above the chondritic point than even the HED isochron. Specifically, the $^{53}Cr/^{52}Cr$ ratio in the VM silicate PB is ~0.63 ε versus ~0.56 ε for the HED PB at a chondritic $^{55}Mn/^{52}Cr$ ratio of ~0.76 (Fig. 8). As a result, the two bulk

isochrons do not intersect near the chondritic point (as would be the expectation if both parent bodies were chondritic), but at a $^{53}Cr/^{52}Cr$ ratio of 0.79 ε and $^{55}Mn/^{52}Cr$ ratio of 1.3.

In the following we will discuss three possible scenarios that can account for the Mn-Cr systematics in the bulk samples of the VM silicates and the HEDs. We present models based on reasonable assumptions for each scenario (Fig. 9) based upon which chronological implications for the differentiation histories of the parent bodies of VM silicates and HEDs and the possibility of a genetic relationship between the two are discussed. The starting point for the models discussed below (and shown in Fig. 9) is defined by the time of solar system formation (T_0) and the corresponding $(^{53}Mn/^{55}Mn)_{0,SSI}$ (or the solar system initial $^{53}Mn/^{55}Mn$ ratio) in region of the solar system where chondrites formed, which are assumed to be 4571 Ma and ~1.4×10^{-5}, respectively. These values are the best estimates of Lugmair and Shukolyukov (1998, 2001) for these parameters. Under the assumption of a gradient in the distribution of ^{53}Mn in the early solar system, suggested by Lugmair and Shukolyukov (1998) and further supported by recently reported results on enstatite chondrites (Shukolyukov and Lugmair, 1999; Shukolyukov and Lugmair, 2003), the $(^{53}Cr/^{52}Cr)_{0,SSI}$ value (or the solar system initial $^{53}Cr/^{52}Cr$ ratio) is assumed to be –0.42 ε. However, it is noted here that the chosen initial values for the $^{53}Mn/^{55}Mn$ ratio (i.e., ~1.4×10^{-5}) and $^{53}Cr/^{52}Cr$ ratio (i.e., ~–0.4 ε) for our model calculations can be arrived at independently of the assumption of a gradient in the ^{53}Mn distribution, simply from the assumption of the solar system age of 4571 Ma and from the ^{53}Mn-^{53}Cr systematics in the angrites. Finally, although we have chosen what we believe to be the best current estimates for the input parameters for the models presented in Fig. 9, the main interpretations based on these models are not critically dependent on the specific values of the parameters indicated above.

5.2.1. Scenario 1: Uniform ^{53}Mn Distribution and Chondritic Mn/Cr Ratio

The simplest interpretation of the Mn-Cr data presented here for the VM silicate clasts arises from the assumptions that the parent bodies of these silicates and the HEDs were close to chondritic in bulk composition and originated in a region of the solar system within which the distribution of ^{53}Mn was uniform. In such a scenario, the Cr isotopic compositions of the bulk silicate reservoirs in these parent bodies would evolve along the same trajectory as that defined by chondrites (solid line in Fig. 9a labeled as "Chondrites/HED-VM PB"). The different slopes and initials of the HED and VM silicate bulk isochrons then imply that these parent bodies underwent global differentiation (i.e., during extensive melting and fractionation in their mantles) at different times. The difference in the timing (T_1'-T_1'') of global differentiation between the parent bodies of the HEDs and the VM silicate clasts is then given by:

$$(T_1'-T_1'') = 1/\lambda \times \{-\ln[(^{53}Mn/^{55}Mn)_{T1''}]/[(^{53}Mn/^{55}Mn)_{T1'}]\} \quad (1)$$

where $(^{53}Mn/^{55}Mn)_{T1'}$ and $(^{53}Mn/^{55}Mn)_{T1''}$ are obtained from the slopes of the isochrons defined by bulk samples of HEDs and VM silicate clasts, respectively. Substituting $(^{53}Mn/^{55}Mn)_{T1'} = (4.7 \pm 0.5) \times 10^{-6}$ and $(^{53}Mn/^{55}Mn)_{T1''} = (3.3 \pm 0.6) \times 10^{-6}$ into equation (1), we estimate (T_1'-T_1'') to be 1.9 ± 1.1 Ma. Comparison with the angrites (which have a ^{53}Mn/^{55}Mn ratio ~1.25×10^{-6} at 4558 Ma; Lugmair and Galer, 1992) then suggests that major silicate differentiation on the VM PB occurred at 4563 Ma (compared to 4565 Ma for a similar event on the HED PB).

Assuming a closed Mn-Cr system since their formation, present day $^{53}Cr/^{52}Cr$ ratios in bulk samples (with varying Mn/Cr ratios) of HEDs and of VM silicate clasts can be estimated from the relationship:

$$(^{53}Cr/^{52}Cr) = (^{53}Cr/^{52}Cr)_{T1} + (^{55}Mn/^{52}Cr)_{sample} \times (^{53}Mn/^{55}Mn)_{T1} \quad (2)$$

where $(^{53}Cr/^{52}Cr)_{T1}$ and $(^{53}Mn/^{55}Mn)_{T1}$ are the initial values of these ratios at the time of global differentiation for each of their parent bodies. For the HED PB, $(^{55}Mn/^{52}Cr)_{sample}$ was taken to range from 0.40 (in Shalka) to 2.46 (in Chervony Kut) (Lugmair and Shukolyukov, 1998). For the VM silicate PB, $(^{55}Mn/^{52}Cr)_{sample}$ ranged from 0.48 (for 4670) to 2.38 (for 4679). Using these ranges of Mn/Cr ratios, the evolution of $^{53}Cr/^{52}Cr$ in HED and VM silicate clast bulk samples is shown in Fig. 9a as the thin dashed and the thick dashed lines, respectively. For comparison, present day measured $^{53}Cr/^{52}Cr$ ratios in bulk samples of Chervony Kut, Shalka, 4670 and 4679 are also shown. The calculated $^{53}Cr/^{52}Cr$ ratios in Chervony Kut and Shalka are ~6 ppm and ~1 ppm lower than the measured values. Moreover, the calculated $^{53}Cr/^{52}Cr$ ratios in the VM silicate clasts are systematically lower than the measured values by ~8 ppm. Given that the external reproducibility of our $^{53}Cr/^{52}Cr$ ratio measurements is of this same order (Table 5), and is more conservative than the $2\sigma_{mean}$ errors on these measurements typically by a factor of ~2, there appears to be a real and systematic difference between the measured and calculated $^{53}Cr/^{52}Cr$ ratios, at least in the case of the Vaca Muerta silicate clasts. This is also reflected in the fact that the $^{53}Cr/^{52}Cr$ ratio (~0.63 ε) at the chondritic Mn/Cr value for the VM bulk isochron lies systematically above the chondritic point (~0.48 ε at 0.76). We, therefore, consider the following two scenarios, which provide a better fit to the data.

5.2.2. Scenario 2: Non-uniform ^{53}Mn Distribution and Chondritic Mn/Cr Ratio

In this scenario, the systematically elevated $^{53}Cr/^{52}Cr$ ratio (relative to chondrites) at a chondritic Mn/Cr ratio (or $(^{55}Mn/^{52}Cr)_{OC}$ ~0.76) for the VM silicate bulk isochron is accounted for by an elevated $^{53}Mn/^{55}Mn$ in the region of the solar system where the VM silicate PB formed, compared to the initial $^{53}Mn/^{55}Mn$ in the region where the ordinary chondrites and the HED PB formed (or $(^{53}Mn/^{55}Mn)_{0,SSI}$, assumed to be ~$1.4 \times 10^{-5}$, as discussed earlier). The bulk Mn/Cr ratios of these parent bodies are assumed to be chondritic and initial $^{53}Cr/^{52}Cr$ ratio is assumed to be the same as well. Then, the initial $(^{53}Mn/^{55}Mn)_{0,VM}$ (or initial $^{53}Mn/^{55}Mn$ in the region where the VM silicates formed) may be determined using the following relationships:

$$(^{53}Cr/^{52}Cr)_{OC/HED} = (^{53}Cr/^{52}Cr)_{0,SSI} + (^{55}Mn/^{52}Cr)_{OC} \times (^{53}Mn/^{55}Mn)_{0,SSI} \quad (3)$$

$$(^{53}Cr/^{52}Cr)_{VM} = (^{53}Cr/^{52}Cr)_{0,SSI} + (^{55}Mn/^{52}Cr)_{OC} \times (^{53}Mn/^{55}Mn)_{0,VM} \quad (4)$$

where $(^{53}Cr/^{52}Cr)_{OC/HED}$ and $(^{53}Cr/^{52}Cr)_{VM}$ are present day ratios in chondrites (~0.48 ε; in this scenario, the present day $^{53}Cr/^{52}Cr$ ratio is assumed to be similar in the HED bulk silicate reservoir) and in the bulk VM silicate PB (~0.63 ε). Substituting these values in the above equations and subtracting (2) from (1) gives the following relationship:

$$(^{53}Mn/^{55}Mn)_{0,VM} = (^{53}Mn/^{55}Mn)_{0,SSI} + (2 \times 10^{-6}) \quad (5)$$

Assuming $(^{53}Mn/^{55}Mn)_{0,SSI}$ ~1.4×10^{-5} at T_0 ~4571 Ma, $(^{53}Mn/^{55}Mn)_{0,VM}$ is estimated to be ~1.6×10^{-5}, and comparison with the slope of the VM bulk isochron ($^{53}Mn/^{55}Mn$ ~3.3×10^{-6}) gives a model age of 4562.5 Ma for global differentiation for the VM silicate PB which, though slightly younger than the model age estimated for scenario 1, is not significantly different from it when the uncertainties are considered. As expected, the model age for global differentiation of the HED PB (from comparison of $(^{53}Mn/^{55}Mn)_{0,SSI}$ with the slope of the HED bulk isochron) gives the same result as in scenario 1 (i.e., 4565 Ma). Figure 9b shows the evolution of $^{53}Cr/^{52}Cr$ in the parent bodies of the HEDs (thin solid line labeled "Chondrites/HED PB") and the VM silicates (thick solid line labeled "VM PB") in such a scenario. Again, present day $^{53}Cr/^{52}Cr$ ratios for selected samples of HEDs (Chervony Kut and Shalka) and VM silicate clasts (4679 and 4670) are calculated and compared with measured values for each. As expected, the fit is no different for the HED samples (for which parameters in scenario 1 and 2 remain the same). However, for the VM clasts, the calculated $^{53}Cr/^{52}Cr$ ratios are within ~2 ppm of the measured values (i.e., well within the smaller $2\sigma_{mean}$ uncertainties). Despite the good fit to the data for VM silicate clasts, however, we consider the possibility of heterogeneous ^{53}Mn distribution in the region where the parent body of these clasts and that of the HEDs formed to be unlikely. The main reason is that ^{53}Mn-^{53}Cr systematics in all other meteorite classes that have so far been investigated (with the exception of enstatite meteorites; Lugmair and Shukolyukov, 1999, 2003) are consistent with having formed within a region in the early solar system where ^{53}Mn was distributed homogenously (Lugmair and Shukolyukov, 1998). There seems to be no a priory reason to believe that VM silicate PB originated in a distinct region characterized by a different ^{53}Mn distribution. In fact, petrologic and geochemical characteristics (e.g., Rubin and Mittlefehldt, 1992) and oxygen isotope systematics (Clayton and Mayeda, 1996) of the mesosiderite clasts

indicate that these materials formed from a geochemical and isotopic reservoir that was similar to that from which the HEDs formed. Finally, the trace element data presented here additionally support the hypothesis that the igneous petrogenetic histories, magma compositions and mantle sources for the VM silicate clasts were generally similar to those for HEDs. Therefore, it would seem reasonable that the HED and VM parent bodies formed within the same narrow region of the solar system characterized by a uniform initial ^{53}Mn as well. Nevertheless, this possibility cannot be ruled out with absolute certainty.

5.3.3. Scenario 3: Uniform ^{53}Mn Distribution and Non-chondritic Mn/Cr Ratio

This last scenario arises from the observations that (1) the HED bulk isochron passes marginally but systematically above the chondritic point and that the VM silicate bulk isochron passes even farther above this point, and (2) these two bulk isochrons intersect at a ^{55}Mn/^{52}Cr ratio of ~1.3 and present day ^{53}Cr/^{52}Cr ratio of 0.79 ε. These observations are consistent with a uniform initial distribution of ^{53}Mn in the region of the early solar system where the parent bodies for HEDs and VM silicates formed (i.e., assuming $(^{53}Mn/^{55}Mn)_{0,SSI}$ ~1.4 × 10^{-5} at T_0 = 4571 Ma, as discussed earlier) and initial accretion of these parent bodies with chondritic bulk Mn/Cr ratios (or $(^{55}Mn/^{52}Cr)_{OC}$ ~0.76), but subsequent evolution of the silicate reservoirs (from which their mantle sources were ultimately established) with an elevated Mn/Cr ratio (i.e., $(^{55}Mn/^{52}Cr)_{VM/HED}$ of ~1.3). In such a scenario, the time (T_1) marking the beginning of global fractionation resulting in the initial increase of the ^{55}Mn/^{52}Cr ratio in the silicate reservoir (from which mantle sources with more extreme Mn/Cr fractionations were ultimately established at time T_2) from chondritic up to ~1.3 may be estimated from the following:

$$(^{53}Cr/^{52}Cr)_{T2} = (^{53}Cr/^{52}Cr)_{0,SSI} + \{(^{55}Mn/^{52}Cr)_{OC} \times (^{53}Mn/^{55}Mn)_{0,SSI} \times [1 - e^{-\lambda(T0-T1)}]\} + \{(^{55}Mn/^{52}Cr)_{VM/HED} \times (^{53}Mn/^{55}Mn)_{T2} \times [e^{\lambda(T1-T2)} - 1]\} \quad (6)$$

where $(^{53}Cr/^{52}Cr)_{T2}$ and $(^{53}Mn/^{55}Mn)_{T2}$ are the initial and slope of the ^{53}Mn-^{53}Cr isochron defined by the bulk samples of the HED PB (subscript T_2') or the VM silicate PB (subscript T_2''). Substituting the values of the various parameters indicated above, we are able to constrain the time of the beginning of global differentiation for the parent bodies of the HEDs and VM silicates (T_1), likely coincident with the time of core formation, to be 4565.6 Ma. This is within ~1 Ma and ~3 Ma of the times at which the mantle source reservoirs of the HEDs (T_2' = 4565 Ma) and the VM silicate clasts (T_2'' = 4563 Ma) were established. Figure 9c shows a model of $^{53}Cr/^{52}Cr$ evolution of a silicate reservoir with chondritic $^{55}Mn/^{52}Cr$ (thin solid line labeled "Chondrites") as well as that of a silicate reservoir with an elevated $^{55}Mn/^{52}Cr$ of ~1.3 that became isolated from the chondritic reservoir at 4565.6 Ma and evolved separately (thick solid line labeled "HED-VM PB"). At times T_2' (4565 Ma) and T_2'' (4563 Ma), the mantle sources in the parent bodies of the HEDs and VM silicate clasts were established from this initially fractionated silicate reservoir. As with our models for previous scenarios, present day $^{53}Cr/^{52}Cr$ ratios for two HEDs (Chervony Kut and Shalka) and two VM silicate clasts (4679 and 4670) with the most extreme Mn/Cr fractionations are also calculated and compared with measured values for each.

As can be seen from Fig. 9, the fit of the calculations to the actual measurements is the best among the three scenarios considered here (specifically, difference between calculated and measured values is –2 ppm for Chervony Kut, +2 ppm for Shalka, and <1 ppm for 4679 and

4670). Given this, it may be reasonable to ask how the $^{55}Mn/^{52}Cr$ ratio in the silicate reservoirs from which the mantle sources for the HEDs and VM clasts were established (assumed here to be ~1.3 from the point of intersection of the HED and VM bulk isochrons; Fig. 8) was elevated beyond the chondritic value. We suggest that segregation of a cumulate or residue comprised primarily of olivine and chromite (having compositions similar to those in main group pallasites) during the magma ocean phase of silicate differentiation might accomplish this elevation of the Mn/Cr ratio in the residual or partial melt compared to the bulk silicate reservoir. We have estimated the bulk Mn/Cr ratio in such a cumulate (or residue) assuming that the relative modal abundances of olivine and chromite are similar to those in main group pallasites (Buseck et al., 1977). For this estimate, we have taken the average concentrations of Mn (2004 μg/g) and Cr (303 μg/g) in main group pallasite olivine from Davis (1977); concentrations of these elements in pallasite chromite are from Bunch and Keil (1971) (Mn ~5092 μg/g and Cr ~43.82 wt.%). Given these constraints, we estimate the $^{55}Mn/^{52}Cr$ ratio of the olivine-chromite cumulate (or residue) to be ~0.47, further implying (with the assumption of a bulk chondritic composition) that the complementary silicate reservoir would have a super-chondritic Mn/Cr ratio.

5.3.4. Chronological Implications

It is noteworthy that no matter which of the above three scenarios is considered, the timing of the *end* of global fractionation processes which established the mantle sources in the HED and the VM silicate parent bodies is not significantly different. Specifically, the models for the three scenarios presented here are all consistent with the end of global differentiation of the HED PB at 4565 Ma, followed by a similar event on the Vaca Muerta PB ~2 Ma later. The fact that

scenario 3 presented above best fits the ^{53}Mn-^{53}Cr data for the HEDs and Vaca Muerta silicate clasts further suggests that the *initiation* of planet-wide differentiation (perhaps coincident with core formation; see below) is likely to have taken place ~1 and ~3 Ma prior to this time for their respective parent bodies. Therefore, comparison with the estimate of the upper limit on the age of the solar system (4571 Ma; Lugmair and Shukolyukov, 1998, 2001) suggests that planetary differentiation on the parent bodies of the HEDs and Vaca Muerta silicates was initiated contemporaneously and occurred ≤6 Ma from the beginning of the solar system. Given that the beginning of planetary-scale differentiation would require an increase in temperature enough to initiate global silicate melting on parent bodies that initially had close to chondritic bulk compositions, it is likely that this event was also associated with the segregation of Fe,Ni-FeS into the core (since the first partial melts in a chondritic system form at <1000°C and consist of Fe,Ni metal and FeS; Kullerud, 1963; Kubaschewski, 1982). The coincidence of the beginning of global differentiation and core formation is supported by the time scale inferred here for the initiation of global differentiation (i.e., ≤6 Ma from the beginning of the solar system) which is consistent with the core formation time scale inferred from ^{182}Hf-^{182}W systematics for asteroidal bodies (Quitté et al., 2000; Kleine et al., 2002; Yin et al., 2002).

It may be reasonable to ask why, if the beginning of global fractionation (and most likely core formation) was contemporaneous on both parent bodies, there was a time lag of ~2 Ma for the end of planet-wide differentiation (and establishment of the mantle source reservoirs with fractionated Mn/Cr) in the two parent bodies. This would be feasible if initiation of differentiation was contemporaneous on both parent bodies, as may be expected for asteroidal bodies of similar bulk composition originating in a narrow region of the solar system and subject to similar heat sources (for example, a similar initial abundance of the short-lived radionuclide

^{26}Al). The difference in the timing of the end of global fractionation processes would then result from slower cooling of the mantle source reservoirs in the VM silicate PB compared to those in the HED PB. Although the reason for this slower cooling of the fractionated mantle reservoirs in the VM silicate PB cannot be rigorously constrained at this time, possibilities may include extended heating (and subsequently a longer time scale for cooling) due to impacts. Finally, one further implication of the ~2 Ma difference between the timing of the end of global fractionation on the parent bodies of the HEDs and VM silicate clasts is that it reinforces the suggestion that the HEDs and the VM silicate clasts did not originate on the same parent body, but on distinct ones that underwent differentiation (and global Mn/Cr fractionation) of their silicate reservoirs independently of each other.

6. SUMMARY AND CONCLUSIONS

We have presented here new data on trace and minor element microdistributions and Cr isotope systematics in selected basaltic and orthopyroxenitic clasts from the VM mesosiderite. The abundances of trace and minor elements in minerals of the basaltic clasts (in order of increasing thermal alteration: pebble 16, 4671, 4695, 4679 and 4677) and in the orthopyroxenitic clast (4659) have allowed us to make the following inferences regarding their crystallization and post-crystallization histories:

1) Following primary igneous crystallization, the basaltic clasts underwent thermal metamorphism under subsolidus conditions that was as severe as that experienced by some of the more highly equilibrated noncumulate eucrites.

2) At the time of metal-silicate mixing (~100-150 Ma after igneous crystallization), the silicate clasts underwent varying degrees of reheating depending on their extent of shielding from hot (likely molten) metal. While some silicate clasts escaped significant reheating (e.g., pebble 16 and 4671), others experienced only sufficient reheating to remelt their mesostasis areas (e.g., 4679, and to a lesser extent, 4695), and yet others experienced extensive reheating and concomitant remelting of mesostasis and non-mesostasis areas (e.g., basaltic clast 4677 and orthopyroxenitic clast 4659). The secondary melts produced due to this reheating reacted with reducing agents such as P (and C?) derived from the metal, resulting in the formation of secondary phases (such as phosphates and pyroxenes).

3) Once the effects of the two major secondary alteration episodes indicated above (i.e., subsolidus metamorphism and secondary magmatic reduction) are taken into account, trace and minor element microdistributions in minerals of the silicate clasts studied here indicate that primary igneous petrogenesis and parent magma compositions of these silicates were broadly similar to those of the eucrites and diogenites.

^{53}Mn-^{53}Cr systematics in two basaltic clasts (pebble 16 and 4671) and two orthopyroxenitic clasts (4659 and 4670) indicate that these clasts are thoroughly equilibrated and that only upper limits on the ^{53}Mn/^{55}Mn ratios may be estimated. The equilibration of Cr isotopes may have taken place either at the time of extensive subsolidus metamorphism or (perhaps more likely) during the metal-silicate mixing event; therefore, this event must have occurred >20 Ma after the beginning of the solar system. The chronological significance of the ^{53}Mn-^{53}Cr systematics in the VM silicate clasts in defining the differentiation history of their parent body arises from the fact that ^{53}Cr excesses in bulk samples of the basaltic clasts (1.01-1.07 ε) are substantially higher than in the orthopyroxenitic clasts (0.53-0.62 ε), and correlate with the Mn/Cr ratios. The bulk

samples of VM silicate clasts define an isochron that indicates a $^{53}Mn/^{55}Mn$ ratio (at the time of last equilibration of Cr isotopes) of $3.3 \pm 0.6 \times 10^{-6}$ and an initial $^{53}Cr/^{52}Cr$ ratio of 0.41 ± 0.08 ε. This is clearly distinct from the slope (corresponding to a $^{53}Mn/^{55}Mn$ ratio of $4.7 \pm 0.5 \times 10^{-6}$) and initial ($0.25 \pm 0.07$ ε) defined by HED bulk samples (Lugmair and Shukolyukov, 1998). Three different scenarios are considered that can account for the Mn-Cr systematics of the VM silicate clasts and the HEDs. In all cases, it is evident that end of planet-wide Mn-Cr fractionation processes in the HED PB preceded a similar event on the VM silicate PB by ~2 Ma. Additionally, the scenario that best fits the data implies that the initiation of differentiation (and likely core formation) on the two parent bodies occurred contemporaneously within ~6 Ma of the beginning of the solar system. Finally, the time difference of ~2 Ma in the establishment of the mantle source reservoirs having fractionated Mn/Cr ratios suggests distinct (but compositionally similar) parent bodies for the HEDs and VM silicate clasts.

*Acknowledgments*¾ We thank those who generously provided us with the samples studied here: thin sections and bulk samples of Vaca Muerta clasts 4659, 4670, 4671, 4677, 4679, and 4695 were made available by the late Dr. Martin Prinz (AMNH); thin section and bulk sample for Vaca Muerta pebble 16 was provided by Dr. Alan Rubin (UCLA). We are extremely grateful to Chris MacIsaac for his invaluable assistance in the clean lab, for measuring the Mn and Cr concentrations and for many helpful suggestions during the course of this work. We thank Mark Robinson and the Center for Planetary Sciences at Northwestern University for access to computing facilities and programming help during preparation of this manuscript. This work has been supported by NASA grants to MW, AMD and GWL, and an NSF grant to MW.

REFERENCES

Agosto W. M., Hewins R. H., and Clarke R. S., Jr. (1980) Allan Hills A77219, the first Antarctic mesosiderite. *Proc. 11th Lunar Planet Sci. Conf.,* 1027-1045.

Anders E. and Grevesse N. (1989) Abundances of the elements: Meteoritic and solar. *Geochim. Cosmochim. Acta* **53,** 197-214.

Begemann F., Weber H. W., Vilcsek E. and Hintenberger H. (1976) Rare gases and ^{36}Cl in stony-iron meteorites: Cosmogenic elemental production rates, exposure ages, diffusion losses and thermal histories. *Geochim. Cosmochim. Acta* **40,** 353-368.

Birck J.-L. and Allègre C. J. (1988) Manganese-chromium isotope systematics and development of the early Solar System. *Nature* **331,** 579-584.

Buchwald V. F. (1975) *Handbook of Iron Meteorites: Their History, Distribution, Composition and Structure.* University of California Press, Berkeley.

Bunch T. E. and Keil K. (1971) Chromite and ilmenite in nonchondritic meteorites. *Am. Mineral.* **56,** 146-157.

Buseck P. R. (1977) Pallasite meteorites – mineralogy, petrology and geochemistry. *Geochim. Cosmochim. Acta* **41,** 711-740.

Clayton R. N. and Mayeda T. K. (1996) Oxygen isotope studies of achondrites. *Geochim. Cosmochim. Acta* **60,** 1999-2017.

Crozaz G., Zinner E., and J. S. Delaney (1985) Rare earth element concentrations of mesosiderite merrillite. *Meteor.* **20,** 629-630.

Davis A. M. (1977) The cosmochemical history of the pallasites. Ph. D. Thesis, Yale Univ.

Delaney J. S., Nehru C. E., and Prinz M. (1980) olivine clasts from mesosiderites and howardites: Clues to the nature of achondrite parent bodies. *Proc. 11th Lunar Planet. Sci. Conf.,* 1073-1087.

Delaney J. S., Nehru C. E., Prinz M., and Harlow G. E. (1981) Metamorphism in mesosiderites. *Proc. 12th Lunar Planet. Sci. Conf.,* 1315-1342.

Delaney J. S., Prinz M., and Takeda H. (1984a) The polymict eucrites. *Proc. 15th Lunar Planet. Sci. Conf.,* C251-C288.

Delaney J. S., O'Neill C., and Prinz M. (1984b) Phosphate minerals in eucrites. *Lunar Planet. Sci. XV,* 208-209 (abstr.).

Floran R. J. (1978) Silicate petrography, classification, and origin of mesosiderites: Review and new observations. *Proc. 9th Lunar Planet. Sci. Conf.,* 1053-1081.

Floss C., Crozaz G., Yamaguchi A., and Keil K. (2000) Trace element constraints on the origins of highly metamorphosed Antarctic eucrites. *Antarct. Meteor. Res.* **13,** 222-237.

Fowler G. W., Shearer C. K., Papike J. J., and Layne G. D. (1995) Diogenites as asteroidal cumulates: Insights from orthopyroxene trace element chemistry. *Geochim. Cosmochim. Acta* **59,** 3071-3084.

Hassanzadeh J., Rubin A. E., and Wasson J. T. (1990) Compositions of large metal nodules in mesosiderites: Links to iron meteorite group IIIAB and the origin of mesosiderite subgroups. *Geochim. Cosmochim. Acta* **54,** 3197-3208.

Harlow G. E., Delaney J. S., Nehru C. E., and Prinz M. (1982) Metamorphic reactions in mesosiderites: Origin of abundant phosphate and silica. *Geochim. Cosmochim. Acta* **46,** 339-348.

Hewins R. H. (1983) impact versus internal origins for mesosiderites. *Proc. 14th Lunar Planet. Sci. Conf., J. Geophys. Res.* **88,** B257-B266.

Ikeda Y., Ebihara M., and Prinz M. (1990) Enclaves in Mt. Padbury and Vaca Muerta mesosiderites: Magmatic and residue (or cumulate) rock types. *Proc. NIPR Symp. Antarct. Meteor.* **3,** 99-131.

Kennedy A. K., Stewart B. W., Hutcheon I. D., Papanastassiou D. A., and Wasserburg G. J. (1992) Partitioning of REE between phosphates and silicates in mesosiderites; Evidence for differing degrees of equilibration. *Lunar Planet. Sci. XXIII*, 681-682 (abstr.).

Kimura M., Ikeda Y., Ebihara M. and Prinz M. (1991) New enclaves in the Vaca Muerta mesosiderite: Petrogenesis and comparison with HED meteorites. *Proc. NIPR Symp. Antarct. Meteor.* **4,** 263-306.

Kleine T., Münker C., Mezger K., and Palme H. (2002) Rapid accretion and early core formation on asteroids and the terrestrial planets from Hf-W chronometry. *Nature* **418,** 952-955.

Kubaschewski O. (1982) *Iron-Binary Phase Diagram.* Springer Verlag.

Kullerud G. (1963) The Fe-Ni-S system. *Ann. Rep. Geophys. Res.* **67,** 4055-4061.

Lugmair G. W. and Shukolyukov A. (1998) Early solar system timescales according to ^{53}Mn-^{53}Cr systematics. *Geochim. Cosmochim. Acta* **62,** 2863-2886.

Lugmair G. W. and Shukolyukov A. (2001) Early solar system events and time scales. *Meteor. Planet. Sci.* **36,** 1017-1026.

McCall G. J. H. (1966) The petrology of Mount Padbury mesosiderite and its achondrite enclaves. *Min. Mag.* **35,** 1029-1060.

MacPherson G. J. and Davis A. M. (1994) Refractory inclusions in the prototypical CM chondrite, Mighei. *Geochim. Cosmochim. Acta* **58,** 5599-5625.

Mittlefehldt D. W. (1979) Petrographic and chemical characterization of igneous lithic clasts from mesosiderites and howardites and comparison with eucrites and diogenites. *Geochim. Cosmochim. Acta* **43,** 1917-1935.

Mittlefehldt D. W. (1990) Petrogenesis of mesosiderites I: Origin of mafic lithologies and comparison with basaltic achondrites. *Geochim. Cosmochim. Acta* **54,** 1165-1173.

Mittlefehldt D. W. (1994) The genesis of diogenites and HED parent body petrogenesis. *Geochim. Cosmochim. Acta* **58,** 1537-1552.

Mittlefehldt D. W., Rubin A. E., and Davis A. M. (1992) Mesosiderite clasts with the most extreme positive europium anomalies among solar system rocks. *Science* **257,** 1096-1099.

Nehru C. E., Zucker S. M., Harlow G. E., and Prinz M. (1980) Olivines and olivine coronas in mesosiderites. *Geochim. Cosmochim. Acta* **44,** 1103-1118.

Prior G. T. (1918) On the mesosiderite-grahamite group of meteorites: With analyses of Vaca Muerta, Hainholz, Simondium, and Powder Mill Creek. *Min. Mag.* **18,** 151-172.

Powell B. N. (1971) Petrology and chemistry of mesosiderites−II. Silicate textures and compositions and metal-silicate relationships. *Geochim. Cosmochim. Acta* **35,** 5-34.

Quitté G., Birck J. L., and Allègre C. J. (2000) ^{182}Hf-^{182}W systematics in eucrites: the puzzle of iron segregation in the early solar system. *Earth Planet. Sci. Lett.* **184,** 83-94.

Rubin A. E. and Jerde E. A. (1987) Diverse eucritic pebbles in the Vaca Muerta mesosiderite. *Earth Planet. Sci. Lett.* **84,** 1-14.

Rubin A. E. and Jerde E. A. (1988) Compositional differences between basaltic and gabbroic clasts in mesosiderites. *Earth Planet. Sci. Lett.* **87,** 485-490.

Rubin A. E. and Mittlefehldt D. W. (1992) Classification of mafic clasts from mesosiderites: Implications for endogenous igneous processes. *Geochim. Cosmochim. Acta* **56,** 827-840.

Scott E. R. D., Haack H., and Love S. G. (2001) Formation of mesosiderites by fragmentation and reaccretion of a large differentiated asteroid. *Meteor. Planet. Sci.* **36,** 869-881.

Shukolyukov A. and Lugmair G. W. (1999) The ^{53}Mn-^{53}Cr isotope systematics of the enstatite chondrites. *Lunar Planet. Sci. XXX,* #1093 (abstr.).

Shukolyukov A. and Lugmair G. W. (2003) Manganese-chromium isotope systematics of the enstatite meteorites. *Geochim. Cosmochim. Acta,* submitted.

Stewart B. W., Papanastassiou D. A., and Wasserburg G. J. (1994) Sm-Nd chronology and petrogenesis of mesosiderites. *Geochim. Cosmochim. Acta* **58,** 3487-3509.

Wasson J. T. and Rubin A. E. (1985) Formation of mesosiderites by low-velocity impacts: A natural consequence of planet formation. *Nature* **318,** 168-170.

Wasson J. T., Schaudy R., Bild R. W., and Chou C.-L. (1974) Mesosiderites-I. Compositions of their metallic portions and possible relationships to other metal-rich meteorite groups. *Geochim. Cosmochim. Acta* **38,** 135-149.

Yamaguchi A., Taylor G. J., Keil K., Floss C., Crozaz G., Nyquist L. E., Bogard D. D., Garrison D., Reese Y., Wiesmann H., and Shih C.-Y. (2001) Post-crystallization reheating and partial melting of eucrite EET90020 by impact into the hot crust of asteroid 4Vesta. *Geochim. Cosmochim. Acta* **65,** 3577-3599.

Yin Q., Jacobsen S. B., Yamashita K., Blichert-Toft J., Télouk P., and Albarède F. (2002) A short timescale for terrestrial planet formation from Hf-W chronometry of meteorites. *Nature* **418,** 949-953.

Figure Captions

Figure 1. Backscattered electron image of the basaltic Vaca Muerta pebble 16. Light gray areas are pyroxenes (pigeonites and augites) and darker gray areas are plagioclase. Although the texture of this clast is generally fine-grained, it is heterogeneous on the mm scale (e.g., the clump of coarser grained pyroxene and plagioclase grains in lower-right section of the image).

Figure 2. Backscattered electron images of the other basaltic Vaca Muerta clasts studied here: (a) 4671 (b) 4695 (c) 4679 and (d) 4677. As in Fig. 1, light gray areas are pyroxenes (Px) and dark gray areas are mostly plagioclase (Pl); areas darker than plagioclase are silica (Si) and the brightest white areas are opaque minerals (Op). "P-rich pockets" in Fig. 2c are fine-grained areas that are enriched in phosphates, silica and opaque minerals compared to the rest of the basaltic matrix.

Figure 3. Backscattered electron images of the two orthopyroxene-rich Vaca Muerta clasts studied here: (a) 4659 and (b) 4670. Light gray areas are olivine (Ol) and the darker gray areas are orthopyroxene (Opx); brightest white areas are opaque minerals (Op).

Figure 4. Range of rare earth element (and yttrium) abundances in minerals of Vaca Muerta basaltic clasts: (a) Pebble 16 (b) 4671 (c) 4695 (d) 4679 and (e) 4677. For comparison, ranges of REE abundances in minerals of noncumulate eucrites are also shown (f) (data from Hsu and Crozaz, 1996; Floss et al., 2000; Yamaguchi et al., 2001); note that phosphates with the lowest REE concentrations and silicate minerals with highest REE concentrations are from the highly

equilibrated eucrites Ibitira, EET90020, or Y86763. All data shown here are normalized to CI-chondritic abundances (Anders and Grevesse, 1989). HREE abundances beyond Gd are not shown for plagioclase in Vaca Muerta clasts since these elements were present in concentrations below the detection limit of the ion microprobe. Errors shown are 1σ from counting statistics only; downward pointing arrows indicate that, in these cases, only upper limits could be estimated (and are shown at the 2σ level).

Figure 5. Range of rare earth element (and yttrium) abundances in merrillite (solid triangles) and orthopyroxene (solid circles) of Vaca Muerta orthopyroxenitic clast 4659. For comparison, the range of REE abundances in diogenitic orthopyroxene (open circles) is also shown (data from Fowler et al., 1995). All data shown here are normalized to CI-chondritic abundances (Anders and Grevesse, 1989). Errors shown are 1σ from counting statistics only; downward pointing arrows indicate that, in these cases, only upper limits could be estimated (and are shown at the 2σ level).

Figure 6. (a) Y vs. La and (b) Sr vs. Na in plagioclases of Vaca Muerta basaltic clasts. (c) Y vs. Ti and (d) Zr vs. Ti in pigeonites of Vaca Muerta basaltic clasts. Symbols for minerals in each of these clasts are as follows: Pebble 16 ●; 4671 ■; 4695 matrix areas ▼; 4679 matrix areas ▲; 4679 P-rich pockets Δ; 4677 ◆. (e) Y Vs. Ti and (f) Zr vs. Ti in the orthopyroxenitic clast 4659 of the Vaca Muerta mesosiderite (solid circles). In (a), (c), and (d), the light gray shaded areas shows compositional ranges of plagioclases in the highly equilibrated noncumulate eucrites Ibitira, EET90020 and Y86763; in (b) the light gray shaded area indicates plagioclase compositions only in EET90020 and Y86763, whereas the dark gray shaded area shows the

compositional range of alkali-depleted plagioclases in Ibitira. Solid line in (a) is the correlation line defined by plagioclases in less equilibrated noncumulate eucrites; dashed line in (b) shows an extension of the trend defined by Ibitira plagioclases. Outlined areas in (b)-(d) indicate the range of compositions in plagioclases or pigeonites of the less equilibrated noncumulate eucrites. Outlined areas in (e)-(f) indicate the compositional range for orthopyroxenes in diogenites. In all figures, the gray arrows schematically illustrate the effects of secondary alteration processes: in (a) and (c)-(f), solid arrows indicate trends resulting from inter-grain equilibration; dashed arrows in (c) and (e) indicate the net loss of Y (and other REEs) in the pyroxenes formed in equilibrium with secondary phosphates resulting from redox reactions. Data for the noncumulate eucrites are from Hsu and Crozaz (1996), Floss et al. (2000) and Yamaguchi et al. (2001); data for diogenites are from Fowler et al. (1995).

Figure 7. ^{53}Mn-^{53}Cr systematics in two basaltic (pebble 16 and 4679) and two orthopyroxene-rich (4659 and 4670) clasts from the Vaca Muerta mesosiderite. ε(53) is as defined in Table 5. All clasts exhibit equilibrated chromium isotopic compositions and, therefore, only upper limits for ^{53}Mn/^{55}Mn can be estimated for each of these clasts. In the case of pebble 16, the internal isochron is the best-fit line to the data; for the other three clasts, the best-fit lines have slightly negative slopes and, therefore, the internal isochrons shown here are slope-zero lines drawn through the average ε(53) value for each clast determined from the chromite ("Chr"), bulk rock ("TR") and silicate ("Sil") fractions. Just as for noncumulate eucrites and diogenites (Lugmair and Shukolyukov, 1998), ^{53}Cr excesses in bulk samples of the basaltic clasts (~1.01 ε in pebble 16; ~1.07 ε in 4679) are significantly higher than in the orthopyroxene-rich clasts (~0.62 ε in 4559; ~0.53 ε in 4670). This suggests that, as in the case of the HED PB, Mn/Cr fractionation in

the Vaca Muerta silicate PB occurred very early in the history of the solar system, when ^{53}Mn was still extant.

Figure 8. ^{53}Mn-^{53}Cr systematics in the parent body of the Vaca Muerta silicate clasts. The measured ^{53}Cr/^{52}Cr ratios for the bulk clasts ("TR" in Fig. 7 and Table 5) are plotted in ε-units versus their respective ^{55}Mn/^{52}Cr ratios. For comparison, the HED bulk isochron corresponding to a ^{55}Mn/^{53}Mn ratio of $(4.7 \pm 0.5) \times 10^{-6}$ and initial ^{53}Cr/^{52}Cr ratio of 0.25 ε (Lugmair and Shukolyukov, 1998) is shown as the dashed line. As seen here, the "TR" data points for the VM clasts define a single isochron that has a distinctly lower slope and higher initial than the HED bulk isochron. Note that the HED and VM bulk isochrons intersect at a ^{53}Cr/^{52}Cr ratio of ~0.79 ε and ^{55}Mn/^{52}Cr ratio of ~1.3.

Figure 9. Cr isotopic evolution in the parent bodies of the Vaca Muerta silicates and HEDs under three different sets of assumptions (scenarios 1, 2 and 3; see text for details). Present day Cr isotopic compositions of the Chervony Kut noncumulate eucrite (CK) and the Shalka diogenite (S) (open squares), and two Vaca Muerta clasts (the basaltic 4579 and the orthopyroxenitic 4670; solid squares) are shown; data for CK and S are from Lugmair and Shukolyukov (1998). T_0 is the time of solar system formation (or addition of live ^{53}Mn to the solar nebula). The absolute values of the ^{53}Cr/^{52}Cr ratios shown in this figure are determined assuming the terrestrial standard value to be 0.1134507 (Lugmair and Shukolyukov, 1998). (a) Scenario 1 assumes a uniform distribution of ^{53}Mn in the region of the solar system where these parent bodies formed and chondritic bulk compositions. T_1' and T_1'' are the times of global Mn/Cr fractionation in the parent bodies of the HEDs and the Vaca Muerta silicates,

respectively. (b) Scenario 2 assumes that while the HED PB originated in the same region of the solar system as ordinary chondrites, the Vaca Muerta silicate PB originated in another region characterized by a slightly higher $^{53}Mn/^{55}Mn$ ratio; the Mn/Cr ratio in these parent bodies, however, are still assumed to be close to chondritic. T_1' and T_1'' are the times of global Mn/Cr fractionation in the parent bodies of the HEDs and the Vaca Muerta silicates, respectively. (c) Scenario 3 assumes that both the parent bodies of the Vaca Muerta silicates and the HEDs originated in the same region of the solar system as ordinary chondrites where the initial $^{53}Mn/^{55}Mn$ was uniform and that both parent bodies initially accreted with chondritic bulk compositions. However, at time T_1, both parent bodies began the process of global differentiation, likely coincident with core formation, and a portion of each of their silicate reservoirs (from which mantle sources of the HEDs and VM clasts were ultimately established) subsequently evolved with an elevated $^{55}Mn/^{52}Cr$ ratio of ~1.3. Time T_2 marks the end of these global fractionation processes when the source reservoirs for the HEDs and Vaca Muerta silicates were finally established; this time was different for the parent bodies of the HEDs (T_2') and the Vaca Muerta silicates (T_2'').

Table 1. Range of rare earth element concentrations (in μg/g) in phosphates of Vaca Muerta clasts.

	Pebble 16				**Clast 4671**			**Clast 4695**		**Clast 4679**		**Clast 4677**		**Clast 4659**	
	Merrillite (4)		Apatite (2)		Merrillite (1)	Apatite (2)		Merrillite (4)		Merrillite (7)		Merrillite (7)		Merrillite (5)	
	(a)*	(b)*	(a)	(b)	(a)	(a)	(b)	(a)	(b)	(a)	(b)	(a)	(b)	(a)	(b)
La	1314 ± 6	1761 ± 7	18.3 ± 0.7	54.7 ± 1.1	2628 ± 5	23.6 ± 0.6	153 ± 1	256 ± 2	1570 ± 5	157 ± 2	1341 ± 6	113 ± 2	248 ± 3	8.80 ± 0.34	13.4 ± 0.5
Ce	3164 ± 15	4022 ± 16	61.0 ± 2.0	143 ± 3	7554 ± 15	78.2 ± 1.8	473 ± 4	664 ± 6	4088 ± 14	400 ± 5	3218 ± 16	258 ± 4	559 ± 6	23.2 ± 0.9	36.5 ± 1.4
Pr	455 ± 7	579 ± 8	8.27 ± 0.95	24.7 ± 1.6	1033 ± 7	14.4 ± 1.0	69.3 ± 1.8	97.8 ± 3.0	617 ± 7	63.0 ± 2.6	492 ± 8	40.3 ± 2.2	78.6 ± 3.1	4.20 ± 0.45	5.19 ± 0.65
Nd	2113 ± 25	2887 ± 28	52.4 ± 3.8	135 ± 6	4141 ± 31	57.3 ± 4.4	309 ± 9	471 ± 15	2764 ± 32	261 ± 8	2197 ± 27	193 ± 8	412 ± 11	11.6 ± 1.7	16.9 ± 2.7
Sm	571 ± 6	862 ± 7	23.3 ± 1.1	46.2 ± 1.5	1032 ± 9	22.6 ± 1.6	83.2 ± 2.7	145 ± 5	798 ± 10	92.2 ± 2.2	696 ± 7	71.6 ± 2.0	138.0 ± 2.9	5.05 ± 0.65	5.26 ± 0.88
Eu	12.8 ± 0.8	11.4 ± 0.9	1.24 ± 0.15	0.74 ± 0.23	18.4 ± 0.9	1.30 ± 0.26	0.90 ± 0.25	9.74 ± 0.81	16.2 ± 1.1	8.70 ± 0.39	16.4 ± 1.0	9.22 ± 0.48	10.5 ± 0.6	2.90 ± 0.30	4.44 ± 0.49
Gd	386 ± 20	345 ± 23	28.1 ± 3.0	31.0 ± 4.6	1038 ± 17	24.3 ± 3.3	79.9 ± 6.4	117 ± 11	705 ± 23	53.3 ± 6.9	538 ± 22	49.9 ± 6.4	84.8 ± 9.0	4.63 ± 1.25	4.2 ± 1.9
Tb	71.2 ± 3.6	84.4 ± 4.2	6.02 ± 0.68	6.70 ± 0.90	172 ± 3	3.66 ± 0.48	15.6 ± 1.0	16.2 ± 1.6	119 ± 3	12.5 ± 1.3	101 ± 4	13.8 ± 1.3	18.2 ± 1.7	1.21 ± 0.21	1.56 ± 0.32
Dy	477 ± 10	772 ± 12	29.6 ± 2.0	50.5 ± 2.7	915 ± 11	19.7 ± 2.0	97.9 ± 3.9	129 ± 6	808 ± 14	90.2 ± 3.8	663 ± 12	124 ± 4	169 ± 5	9.2 ± 1.2	13.0 ± 1.8
Y	1997 ± 9	5069 ± 17	166 ± 3	277 ± 4	4303 ± 10	119 ± 2	533 ± 4	664 ± 6	4533 ± 13	546 ± 6	3735 ± 16	801 ± 7	1139 ± 9	57.2 ± 1.2	82.8 ± 1.9
Ho	99.7 ± 3.1	167 ± 4	6.25 ± 0.69	9.24 ± 0.83	167 ± 2	3.90 ± 0.44	17.8 ± 0.8	29.0 ± 1.4	154 ± 3	17.7 ± 1.2	124 ± 4	26.3 ± 1.4	40.1 ± 1.9	1.68 ± 0.24	2.90 ± 0.40
Er	240 ± 5	400 ± 7	16.2 ± 1.2	20.2 ± 1.4	450 ± 8	8.6 ± 1.4	52.4 ± 2.9	68.4 ± 4.7	411 ± 10	47.4 ± 2.2	324 ± 6	74.8 ± 2.6	101 ± 3	7.59 ± 0.89	11.2 ± 1.4
Tm	31.3 ± 1.0	50.7 ± 1.2	1.84 ± 0.23	2.52 ± 0.26	49.4 ± 0.8	1.48 ± 0.17	5.95 ± 0.28	10.8 ± 0.6	51.9 ± 1.0	6.14 ± 0.45	39.8 ± 1.2	9.18 ± 0.56	12.3 ± 0.7	1.34 ± 0.15	1.66 ± 0.22
Yb	215 ± 8	387 ± 10	10.9 ± 1.6	15.8 ± 2.0	271 ± 7	4.2 ± 1.4	34.2 ± 2.9	62.7 ± 5.1	307 ± 10	50.3 ± 3.1	266 ± 9	72.8 ± 3.5	94.1 ± 4.4	9.0 ± 1.0	12.2 ± 1.5

*(a) = phosphate with the lowest REE abundances; (b) = phosphate with the highest REE abundances.
Errors are 1σ from counting statistics only. Number of analyses are given in parentheses.

Table 2. Range of trace element concentrations (in μg/g) in plagioclase of Vaca Muerta basaltic clasts.

	Pebble 16 (2)		**Clast 4671** (2)		**Clast 4695** (2)		**Clast 4679** (2)		**Clast 4677** (2)	
	(a)*	(b)*	(a)	(b)	(a)	(b)	(a)	(b)	(a)	(b)
La	0.885 ± 0.028	1.13 ± 0.03	1.48 ± 0.05	1.87 ± 0.06	2.02 ± 0.06	2.77 ± 0.07	1.35 ± 0.03	1.37 ± 0.04	0.221 ± 0.013	0.646 ± 0.023
Ce	1.80 ± 0.06	2.11 ± 0.07	3.18 ± 0.12	3.64 ± 0.12	4.00 ± 0.13	6.51 ± 0.18	2.54 ± 0.07	2.66 ± 0.08	0.317 ± 0.026	0.984 ± 0.046
Pr	0.213 ± 0.028	0.353 ± 0.036	0.370 ± 0.050	0.424 ± 0.052	0.549 ± 0.060	0.743 ± 0.072	0.275 ± 0.031	0.240 ± 0.031	0.031 ± 0.010	0.077 ± 0.017
Nd	0.560 ± 0.073	0.889 ± 0.090	1.15 ± 0.20	1.56 ± 0.22	1.29 ± 0.21	3.33 ± 0.35	1.11 ± 0.10	1.03 ± 0.10	0.101 ± 0.032	0.341 ± 0.057
Sm	0.225 ± 0.034	0.380 ± 0.039	0.22 ± 0.12	<0.20	0.24 ± 0.11	0.85 ± 0.15	0.239 ± 0.036	0.324 ± 0.039	0.095 ± 0.030	0.101 ± 0.031
Eu	1.50 ± 0.04	1.55 ± 0.04	1.31 ± 0.09	1.61 ± 0.09	1.37 ± 0.09	1.39 ± 0.09	1.50 ± 0.04	1.52 ± 0.04	1.09 ± 0.03	1.27 ± 0.04
Gd	0.299 ± 0.048	0.232 ± 0.057	<0.11	0.54 ± 0.12	0.12 ± 0.10	0.50 ± 0.19	0.196 ± 0.055	0.140 ± 0.053	0.057 ± 0.019	0.063 ± 0.029
Y	0.433 ± 0.028	0.441 ± 0.028	0.579 ± 0.046	0.684 ± 0.047	0.502 ± 0.042	2.338 ± 0.093	0.418 ± 0.027	0.529 ± 0.032	0.096 ± 0.013	0.149 ± 0.016
Na	7993 ± 7	8299 ± 7	7831 ± 9	6842 ± 8	7179 ± 9	7226 ± 9	8623 ± 7	8699 ± 7	8455 ± 7	8039 ± 7
K	481 ± 2	382 ± 2	400 ± 3	366 ± 2	481 ± 3	406 ± 3	391 ± 2	470 ± 2	370 ± 2	328 ± 2
Sr	212 ± 1	227 ± 1	212 ± 1	221 ± 1	206 ± 1	208 ± 1	228 ± 1	221 ± 1	217 ± 1	212 ± 1
Ba	78.8 ± 0.6	85.2 ± 0.6	73.8 ± 0.6	84.7 ± 0.6	77.0 ± 0.6	84.2 ± 0.7	89.9 ± 0.6	87.9 ± 0.7	82.7 ± 0.6	86.4 ± 0.6

*(a) = plagioclase with the lowest REE abundances; (b) = plagioclase with the highest REE abundances.
Errors are 1σ from counting statistics only; upper limits are 2σ. Number of analyses are given in parentheses. Abundances of heavy REE (beyond Gd) are not given since they are below the detection limit.

Table 3. Range of rare earth element concentrations (in μg/g) in augites of Vaca Muerta basaltic clasts.

	Pebble 16 (3)		**Clast 4671** (7)		**Clast 4695** (2)		**Clast 4679** (4)		**Clast 4677** (1)
	(a)*	(b)*	(a)	(b)	(a)	(b)	(a)	(b)	
La	0.116 ± 0.011	0.169 ± 0.015	0.339 ± 0.022	0.383 ± 0.028	0.137 ± 0.015	2.01 ± 0.06	0.149 ± 0.011	0.238 ± 0.015	0.265 ± 0.025
Ce	0.585 ± 0.038	0.763 ± 0.050	1.71 ± 0.08	2.42 ± 0.11	0.800 ± 0.056	6.76 ± 0.17	0.846 ± 0.043	1.56 ± 0.06	0.510 ± 0.055
Pr	0.164 ± 0.025	0.215 ± 0.032	0.424 ± 0.049	0.600 ± 0.068	0.248 ± 0.038	1.33 ± 0.09	0.265 ± 0.029	0.372 ± 0.037	0.080 ± 0.028
Nd	0.92 ± 0.14	1.19 ± 0.18	2.61 ± 0.28	3.70 ± 0.40	1.51 ± 0.22	6.58 ± 0.47	1.42 ± 0.16	2.56 ± 0.23	0.374 ± 0.097
Sm	0.563 ± 0.060	0.813 ± 0.083	1.78 ± 0.13	2.24 ± 0.17	0.97 ± 0.10	2.29 ± 0.16	0.896 ± 0.069	1.83 ± 0.11	0.233 ± 0.034
Eu	0.027 ± 0.009	0.014 ± 0.010	0.042 ± 0.012	0.038 ± 0.014	0.022 ± 0.009	0.101 ± 0.030	0.043 ± 0.009	0.040 ± 0.013	0.057 ± 0.010
Gd	1.25 ± 0.12	0.87 ± 0.17	3.33 ± 0.25	3.12 ± 0.30	1.45 ± 0.17	2.58 ± 0.31	1.05 ± 0.15	2.69 ± 0.22	0.366 ± 0.079
Tb	0.273 ± 0.022	0.312 ± 0.031	0.646 ± 0.042	0.721 ± 0.053	0.394 ± 0.033	0.618 ± 0.052	0.322 ± 0.026	0.580 ± 0.037	0.104 ± 0.022
Dy	2.49 ± 0.16	2.94 ± 0.20	5.02 ± 0.28	5.01 ± 0.33	3.00 ± 0.22	3.53 ± 0.26	2.69 ± 0.16	4.21 ± 0.22	0.721 ± 0.083
Y	12.9 ± 0.2	17.2 ± 0.2	27.3 ± 0.3	27.5 ± 0.3	16.7 ± 0.2	26.0 ± 0.3	15.6 ± 0.2	27.8 ± 0.2	4.52 ± 0.15
Ho	0.489 ± 0.034	0.619 ± 0.045	1.10 ± 0.06	1.15 ± 0.08	0.627 ± 0.049	0.846 ± 0.060	0.582 ± 0.035	0.954 ± 0.050	0.186 ± 0.034
Er	1.66 ± 0.11	1.99 ± 0.14	3.21 ± 0.19	3.43 ± 0.23	2.19 ± 0.16	2.19 ± 0.18	1.67 ± 0.11	2.79 ± 0.15	0.617 ± 0.061
Tm	0.247 ± 0.016	0.276 ± 0.019	0.413 ± 0.025	0.485 ± 0.032	0.320 ± 0.023	0.418 ± 0.027	0.285 ± 0.016	0.405 ± 0.021	0.102 ± 0.016
Yb	1.88 ± 0.12	2.10 ± 0.16	2.68 ± 0.19	3.21 ± 0.23	2.39 ± 0.17	2.01 ± 0.18	1.89 ± 0.12	2.65 ± 0.17	0.823 ± 0.090

*(a) = augite with the lowest REE abundances; (b) = augite with the highest REE abundances.
Errors are 1σ from counting statistics only. Number of analyses are given in parentheses.

Table 4. Ranges of element concentrations (in μg/g, unless noted otherwise), molar Fe/Mn and Fe/Mg, and mg# (atomic Mg/Mg+Fe) in low-Ca pyroxenes of Vaca Muerta clasts.

	Pebble 16		**Clast 4671**		**Clast 4695**		**Clast 4679**		**Clast 4677**		**Clast 4659**	
	Pigeonite (8)		Pigeonite (5)		Pigeonite (7)		Pigeonite (12)		Pigeonite (5)		Orthopyroxene (8)	
	(a)*	(b)*	(a)	(b)	(a)	(b)	(a)	(b)	(a)	(b)	(a)	(b)
La	0.033 ± 0.008	0.176 ± 0.019	0.028 ± 0.005	0.070 ± 0.008	0.014 ± 0.004	0.057 ± 0.009	0.009 ± 0.003	0.166 ± 0.012	0.068 ± 0.011	0.063 ± 0.012	0.004 ± 0.003	0.014 ± 0.004
Ce	0.131 ± 0.026	0.647 ± 0.058	0.160 ± 0.020	0.347 ± 0.028	0.075 ± 0.016	0.379 ± 0.036	0.023 ± 0.006	0.583 ± 0.036	0.086 ± 0.019	0.389 ± 0.049	<0.004	0.015 ± 0.007
Pr	0.084 ± 0.027	0.129 ± 0.033	0.066 ± 0.016	0.099 ± 0.018	0.021 ± 0.010	0.097 ± 0.022	0.013 ± 0.006	0.148 ± 0.024	0.014 ± 0.010	0.074 ± 0.028	<0.006	0.018 ± 0.009
Nd	0.228 ± 0.072	0.604 ± 0.115	0.283 ± 0.079	0.678 ± 0.111	0.241 ± 0.084	0.601 ± 0.129	<0.023	0.922 ± 0.094	0.139 ± 0.050	0.244 ± 0.081	<0.022	<0.039
Sm	0.316 ± 0.036	0.427 ± 0.042	0.229 ± 0.039	0.445 ± 0.051	0.179 ± 0.040	0.307 ± 0.053	0.030 ± 0.012	0.622 ± 0.034	0.051 ± 0.013	0.190 ± 0.032	0.047 ± 0.021	0.044 ± 0.018
Eu	0.047 ± 0.009	0.024 ± 0.006	0.007 ± 0.004	0.007 ± 0.005	0.006 ± 0.005	0.026 ± 0.011	0.012 ± 0.004	0.039 ± 0.007	0.034 ± 0.006	0.053 ± 0.011	<0.004	0.014 ± 0.006
Gd	0.601 ± 0.086	0.942 ± 0.109	0.472 ± 0.079	0.497 ± 0.118	0.424 ± 0.084	0.935 ± 0.123	0.035 ± 0.016	0.880 ± 0.074	0.161 ± 0.041	0.266 ± 0.071	0.033 ± 0.023	0.105 ± 0.035
Tb	0.163 ± 0.024	0.165 ± 0.026	0.144 ± 0.016	0.213 ± 0.021	0.116 ± 0.016	0.222 ± 0.023	0.005 ± 0.002	0.208 ± 0.020	0.018 ± 0.008	0.066 ± 0.018	0.007 ± 0.004	0.029 ± 0.007
Dy	1.22 ± 0.10	1.53 ± 0.11	1.34 ± 0.12	1.72 ± 0.13	0.952 ± 0.118	1.86 ± 0.16	0.041 ± 0.018	1.77 ± 0.08	0.236 ± 0.041	0.495 ± 0.071	0.044 ± 0.027	0.108 ± 0.037
Y	7.67 ± 0.18	10.3 ± 0.2	8.48 ± 0.13	12.1 ± 0.1	7.60 ± 0.15	12.8 ± 0.2	0.424 ± 0.025	12.1 ± 0.1	1.46 ± 0.07	3.46 ± 0.13	0.077 ± 0.015	0.781 ± 0.043
Ho	0.303 ± 0.040	0.306 ± 0.040	0.316 ± 0.028	0.383 ± 0.029	0.319 ± 0.033	0.426 ± 0.037	0.028 ± 0.007	0.362 ± 0.029	0.081 ± 0.019	0.196 ± 0.035	<0.003	0.042 ± 0.011
Er	1.20 ± 0.08	1.43 ± 0.09	1.24 ± 0.09	1.49 ± 0.10	0.870 ± 0.091	1.62 ± 0.12	0.084 ± 0.020	1.47 ± 0.06	0.281 ± 0.035	0.605 ± 0.062	0.029 ± 0.018	0.087 ± 0.027
Tm	0.201 ± 0.021	0.226 ± 0.022	0.193 ± 0.014	0.242 ± 0.015	0.157 ± 0.015	0.270 ± 0.019	0.018 ± 0.004	0.218 ± 0.015	0.032 ± 0.008	0.126 ± 0.019	0.005 ± 0.003	0.018 ± 0.005
Yb	1.42 ± 0.11	1.41 ± 0.11	1.45 ± 0.11	1.88 ± 0.12	1.25 ± 0.11	2.07 ± 0.14	0.112 ± 0.024	1.57 ± 0.08	0.539 ± 0.061	0.998 ± 0.099	0.016 ± 0.015	0.185 ± 0.041
Mg	6.45%	6.51%	6.58%	6.27%	6.62%	6.55%	7.92%	6.45%	7.92%	7.26%	15.2%	15.8%
Al	1400 ± 3	1755 ± 4	1528 ± 2	1903 ± 2	1853 ± 3	2801 ± 4	1543 ± 2	2509 ± 3	1562 ± 3	2895 ± 5	2799 ± 4	4166 ± 4
Ti	1587 ± 17	2172 ± 20	1672 ± 12	2095 ± 13	1797 ± 15	2512 ± 18	1497 ± 10	2165 ± 13	1491 ± 16	3300 ± 28	1943 ± 16	636 ± 8
Mn	7504 ± 13	7387 ± 13	7240 ± 9	7234 ± 8	7718 ± 11	7151 ± 10	8147 ± 8	7017 ± 8	8506 ± 13	7311 ± 15	4589 ± 9	3847 ± 7
Fe	27.7%	27.3%	27.4%	27.3%	27.2%	25.6%	25.1%	24.4%	24.9%	22.8%	14.1%	12.3%
Zr	14.3 ± 0.4	17.4 ± 0.4	12.3 ± 0.3	21.5 ± 0.3	17.3 ± 0.4	38.2 ± 0.5	4.06 ± 0.12	34.2 ± 0.4	17.0 ± 0.4	45.0 ± 0.8	2.55 ± 0.14	0.836 ± 0.072
Hf	0.84 ± 0.11	0.92 ± 0.12	<0.11	0.73 ± 0.16	0.519 ± 0.139	1.34 ± 0.20	0.275 ± 0.049	1.56 ± 0.09	0.722 ± 0.075	1.25 ± 0.12	0.154 ± 0.052	<0.04
Fe/Mn	36	36	37	37	35	35	30	34	29	31	30	31
Fe/Mg	1.87	1.83	1.81	1.90	1.79	1.70	1.38	1.65	1.37	1.37	0.40	0.34
mg#	0.35	0.35	0.36	0.35	0.36	0.37	0.42	0.38	0.42	0.42	0.71	0.75

*(a) = low-Ca pyroxene with the lowest REE abundances; (b) = low-Ca pyroxene with the highest REE abundances.

Errors are 1σ from counting statistics only; upper limits are 2σ. In case of the major elements Mg and Fe, errors are <0.2%. Number of analyses are given in parentheses.

Table 5. Manganese and chromium concentrations, Mn/Cr ratios, and ^{53}Cr excesses in Vaca Muerta clasts.

Sample*	Weight (mg)	Mn (μg/g)	Cr (μg/g)	$^{55}Mn/^{52}Cr$ (±5%)	ε(53)†
Pebble 16 TR	236.1‡	4614	2605	2.00	1.01 ± 0.08
Pebble 16 Chr	n.d.	—	—	0.011	0.94 ± 0.09
Pebble 16 Sil	~236	5110	981	5.88	1.03 ± 0.10
4679 TR	319.3‡	5214	2479	2.38	1.07 ± 0.10
4679 Chr	n.d.	—	—	0.014	1.08 ± 0.07
4679 Sil	~319	4860	961	5.71§	1.07 ± 0.09
4659 TR	278.1‡	3896	6683	0.66	0.62 ± 0.07
4659 Chr	n.d.	—	—	0.020	0.59 ± 0.09
4659 Sil	~278	3809	1524	2.82	0.56 ± 0.12
4670 TR	249.3‡	3915	9141	0.48	0.53 ± 0.09
4670 Chr	n.d.	—	—	0.016	0.57 ± 0.08
4670 Sil	~249	3669	2197	1.89	0.55 ± 0.09

*TR = whole-rock; Chr = chromite; Sil = silicate.

†$\varepsilon(53) = [(^{53}Cr/^{52}Cr)_{sample}/(^{53}Cr/^{52}Cr)_{standard} - 1] \times 10^4$, where $(^{53}Cr/^{52}Cr)_{standard}$ is taken to be 0.1134507 (Lugmair and Shukolyukov, 1998); the uncertainties on ε(53) are based on estimates of the reproducibility of repeat measurements (see text for more details).

‡After fractional dissolution of a bulk sample, equal proportions of the obtained solutions for silicate (Sil) and chromite (Chr) were recombined to produce a representative whole-rock (TR) solution.

§Uncertainty on this $^{55}Mn/^{52}Cr$ ratio is ±10%.

n.d. = not determined.

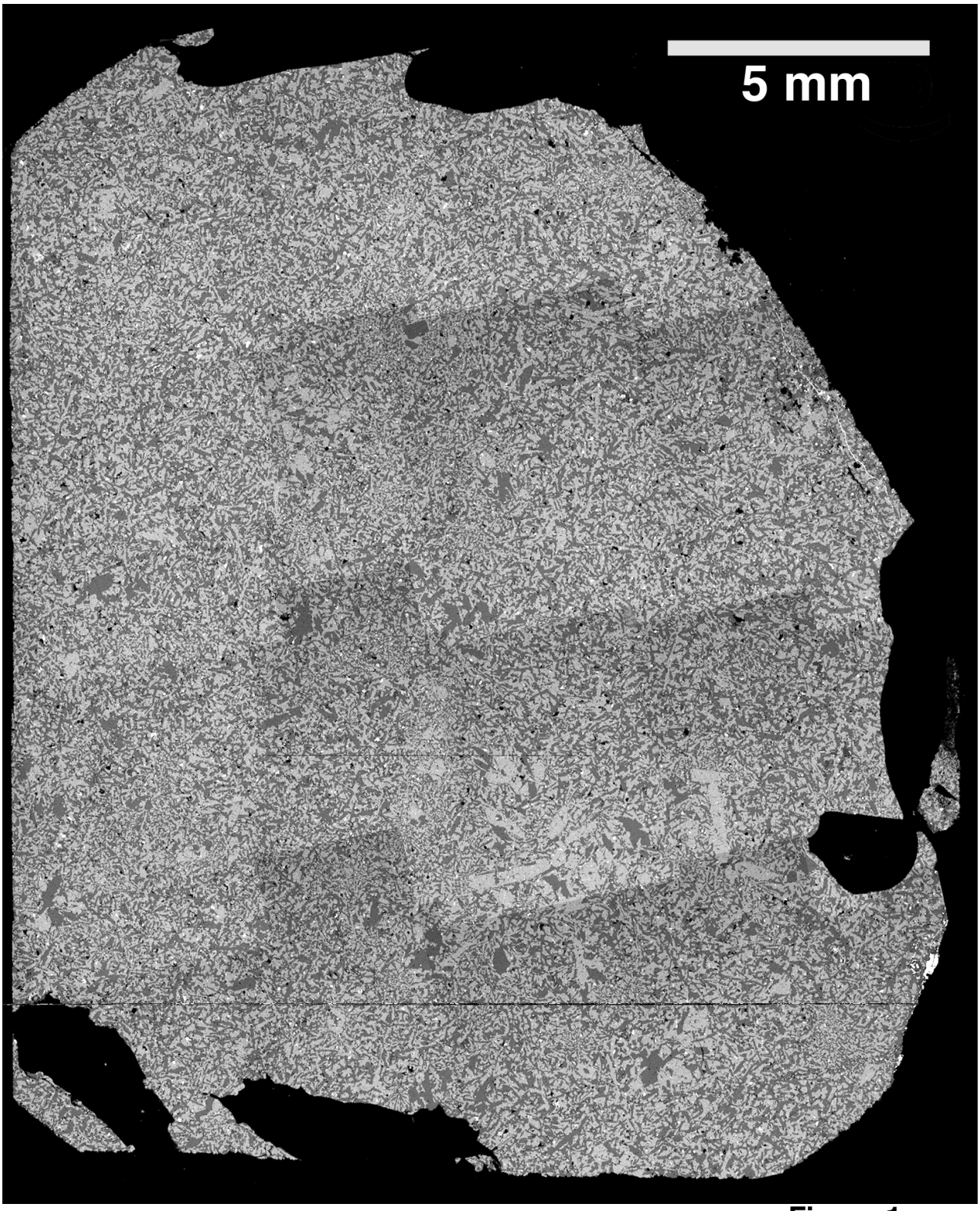

Figure 1
Wadhwa et al.

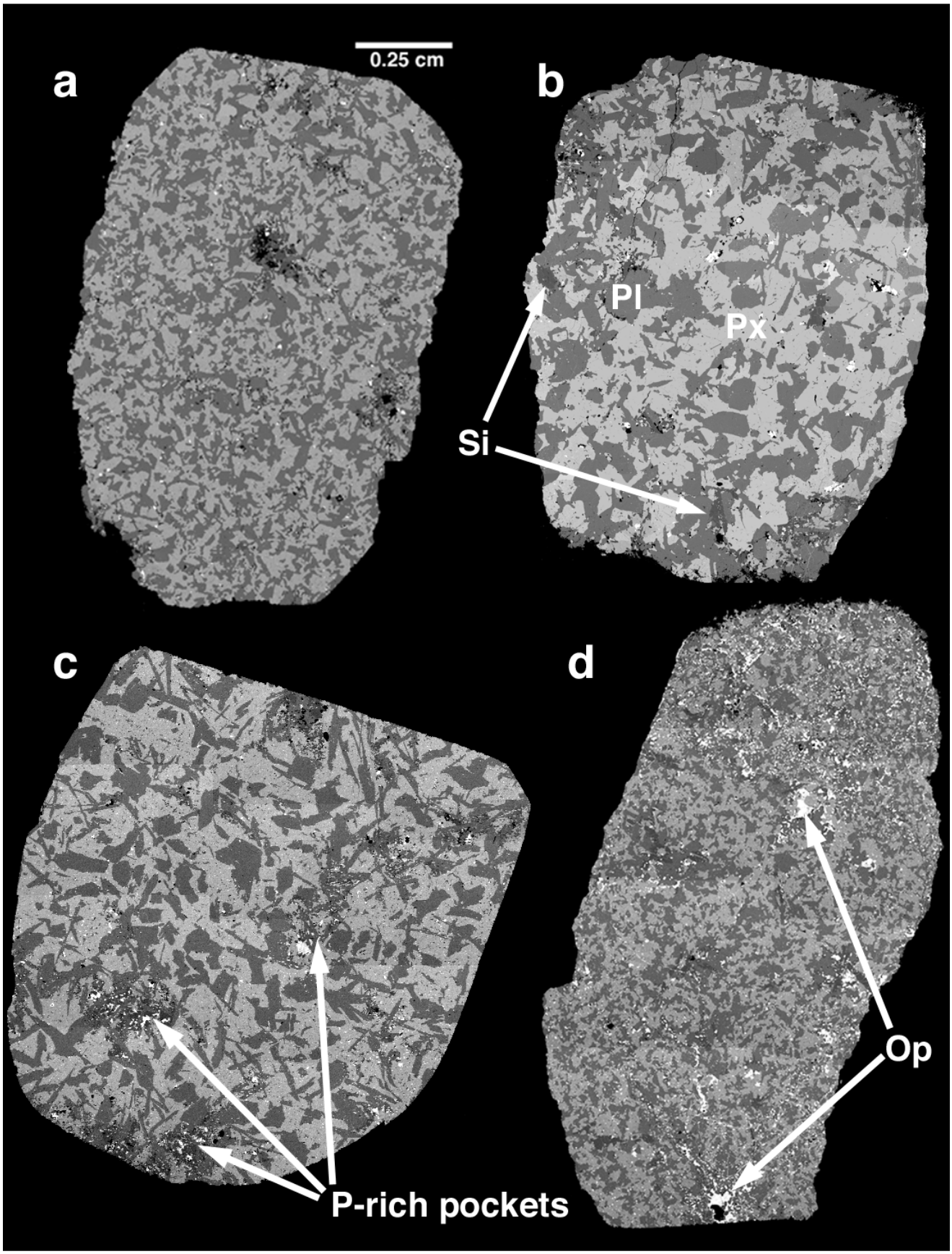

Figure 2
Wadhwa et al.

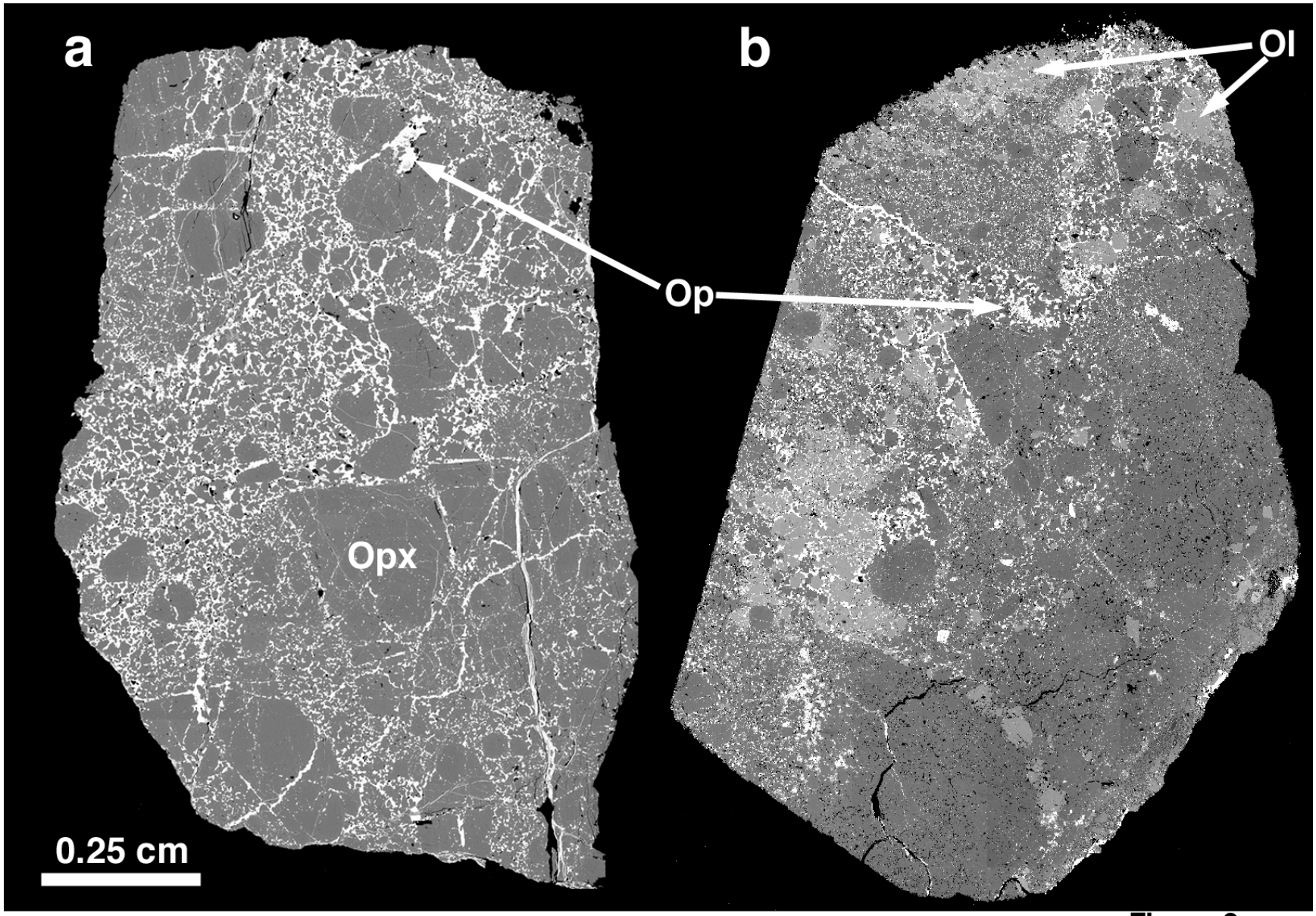

Figure 3
Wadhwa et al.

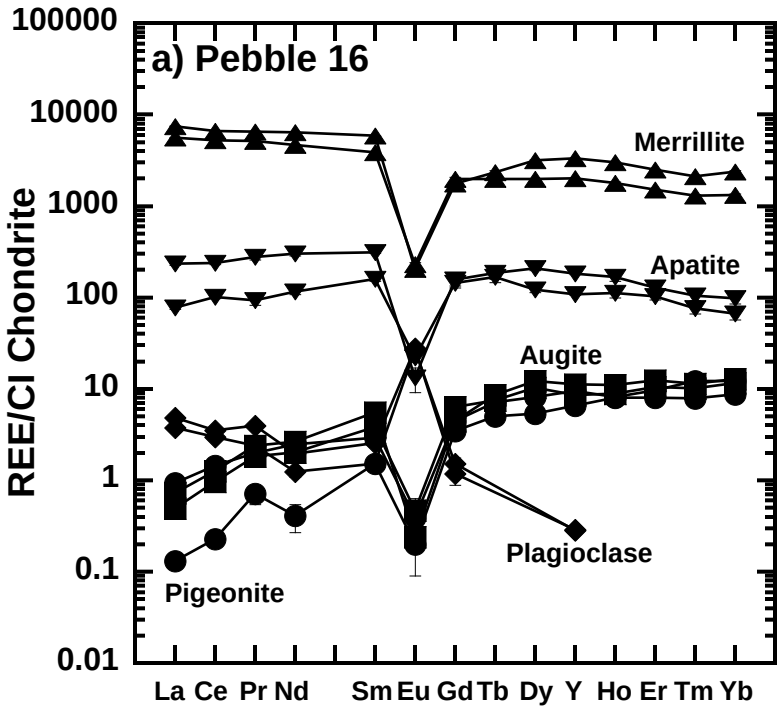

Figure 4a
Wadhwa et al.

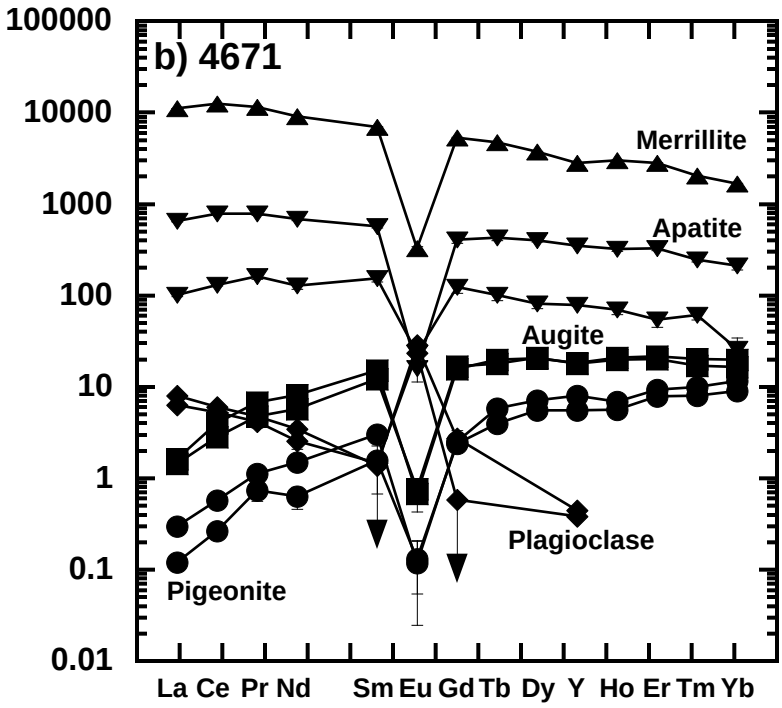

Figure 4b
Wadhwa et al.

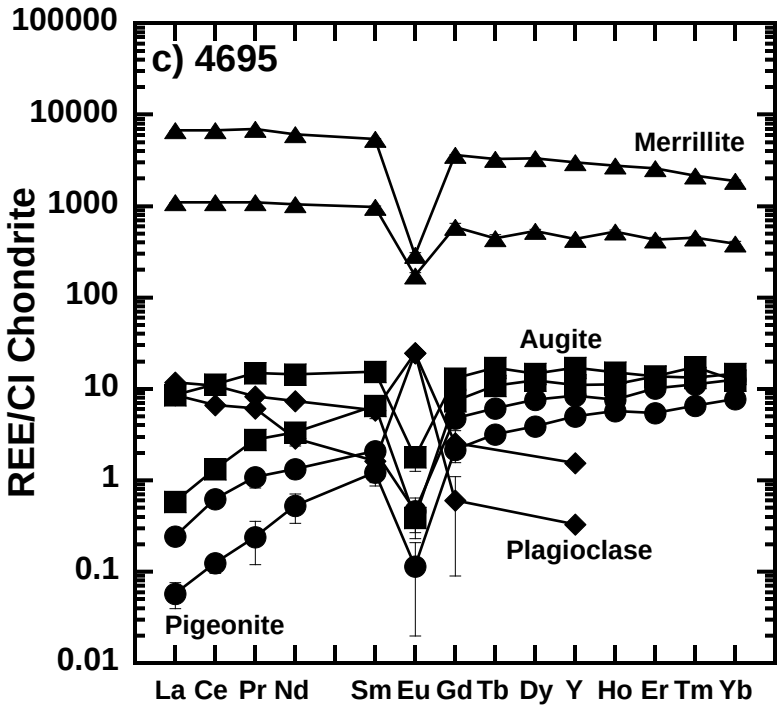

Figure 4c
Wadhwa et al.

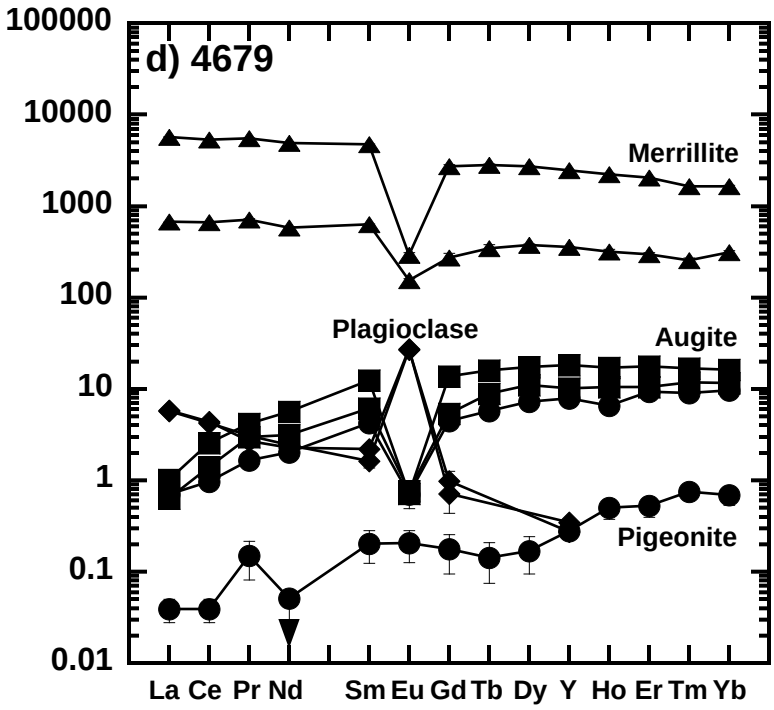

Figure 4d
Wadhwa et al.

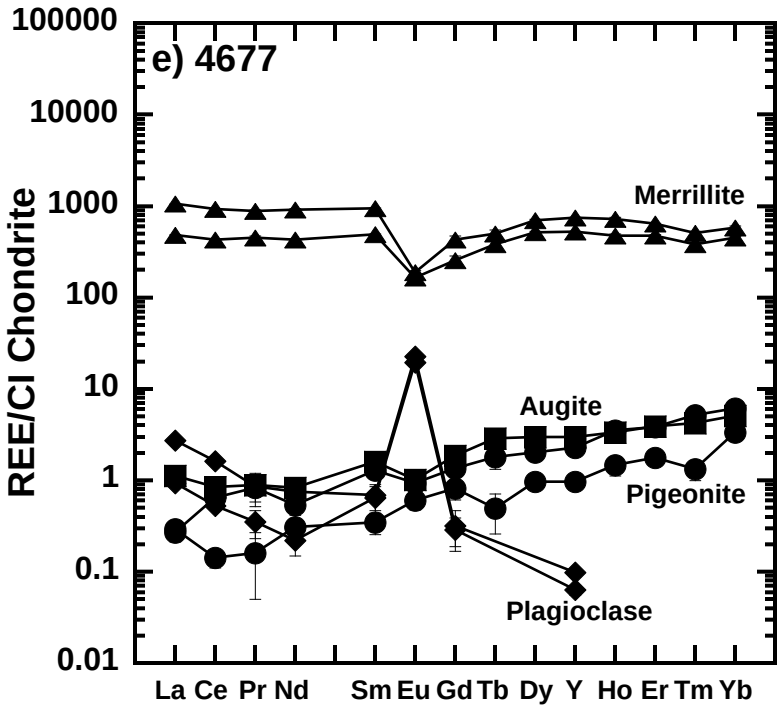

Figure 4e
Wadhwa et al.

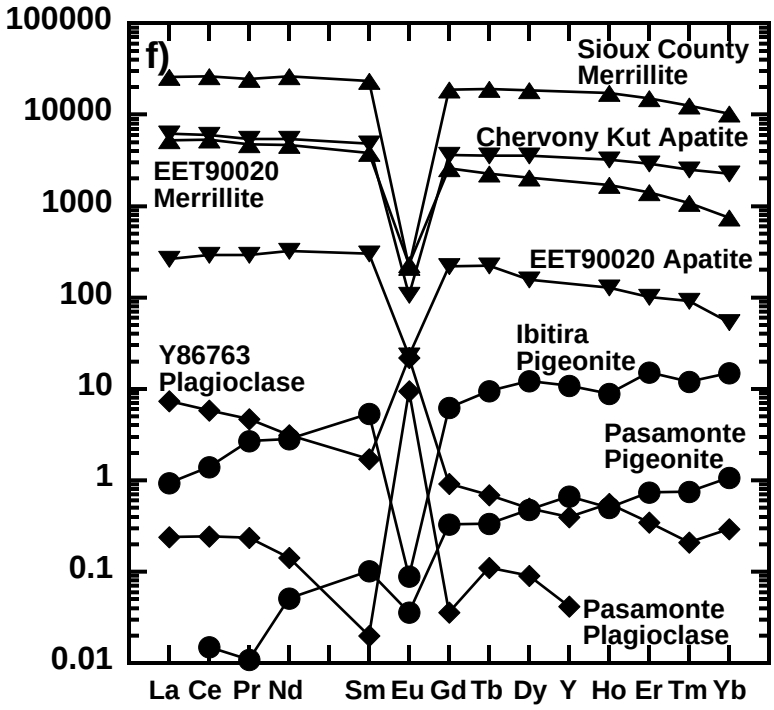

Figure 4f
Wadhwa et al.

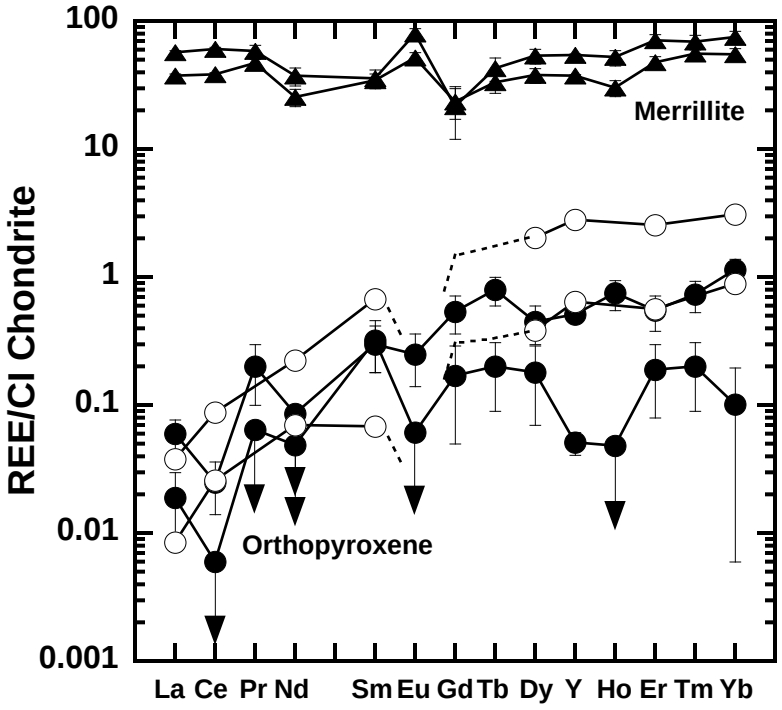

Figure 5
Wadhwa et al.

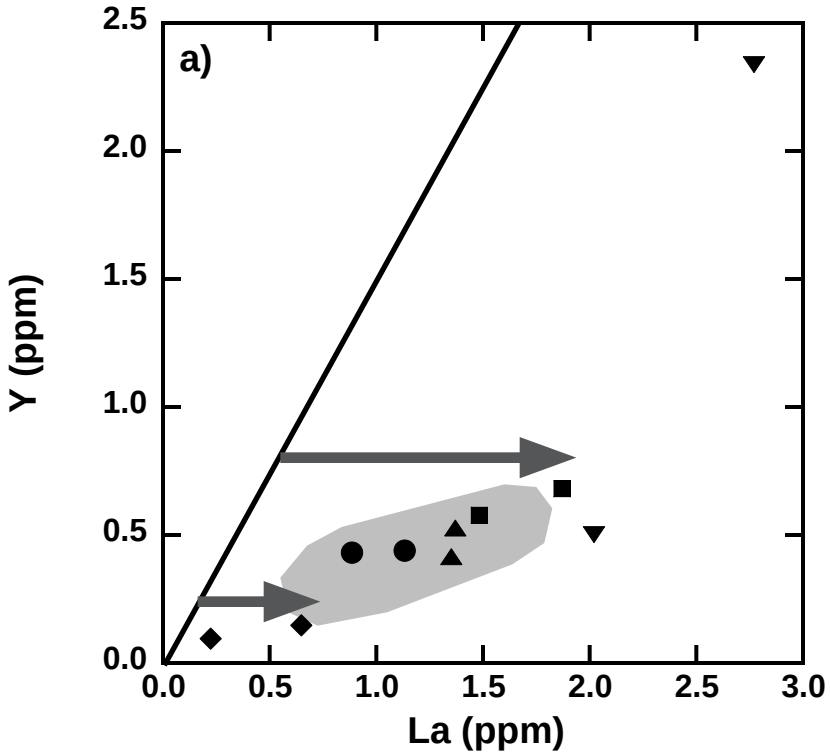

Figure 6a
Wadhwa et al.

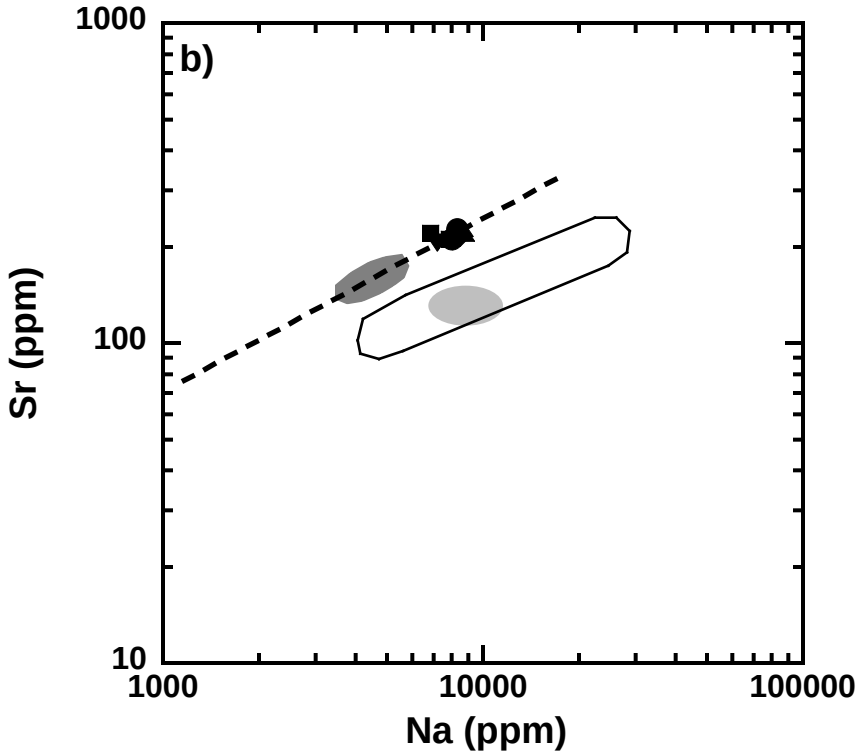

Figure 6b
Wadhwa et al.

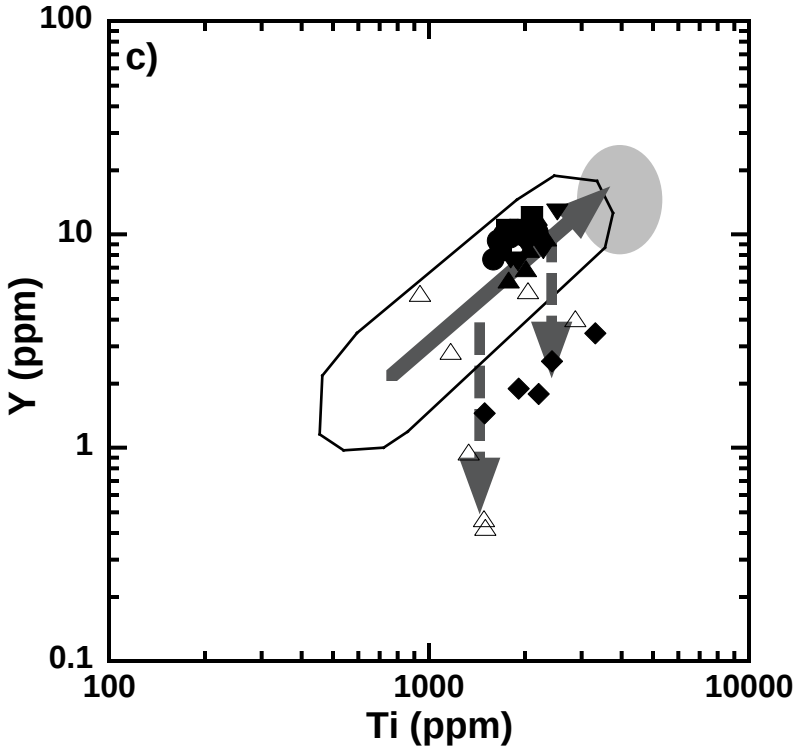

Figure 6c
Wadhwa et al.

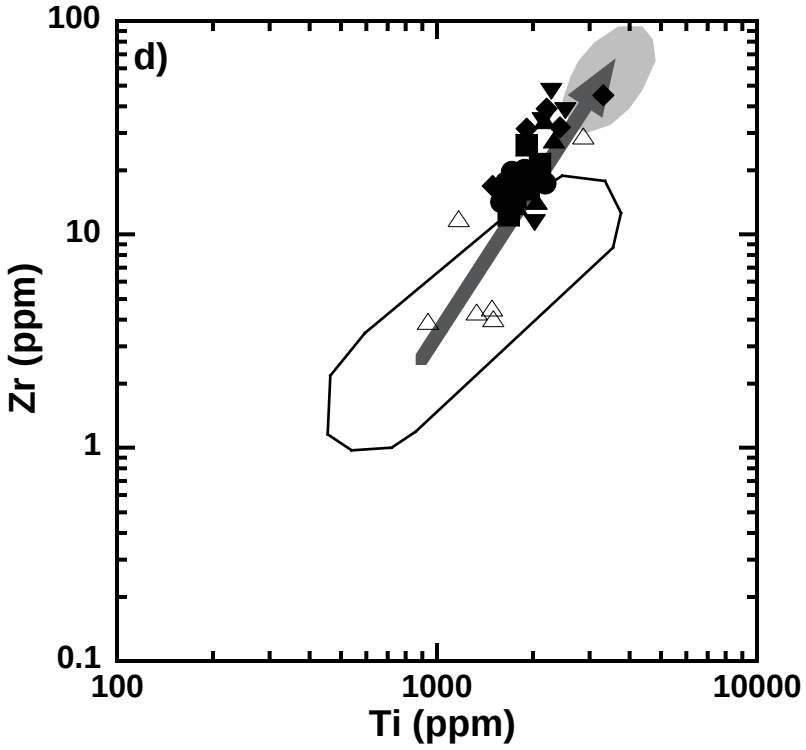

Figure 6d
Wadhwa et al.

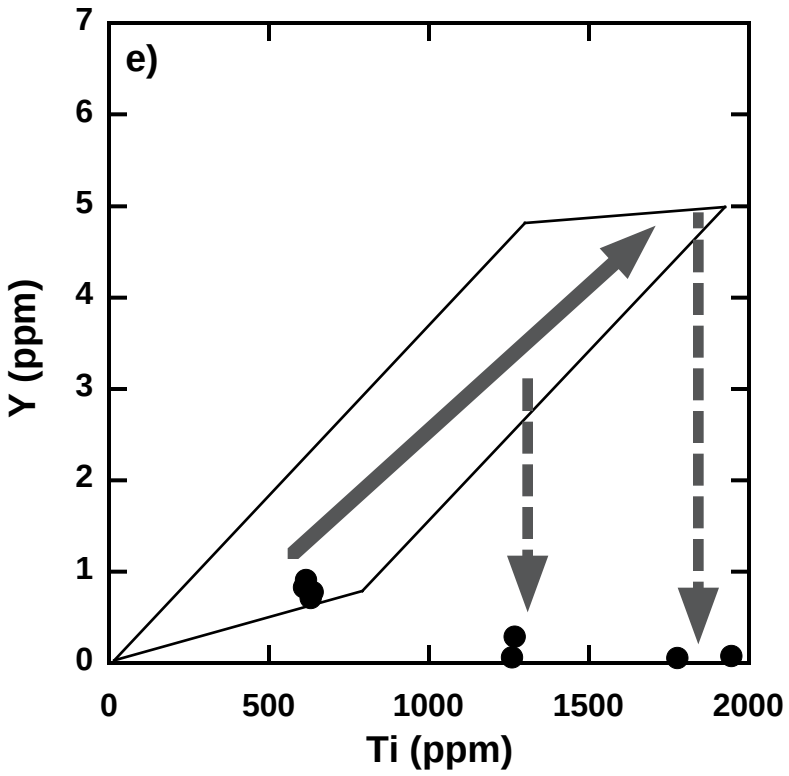

Figure 6e
Wadhwa et al.

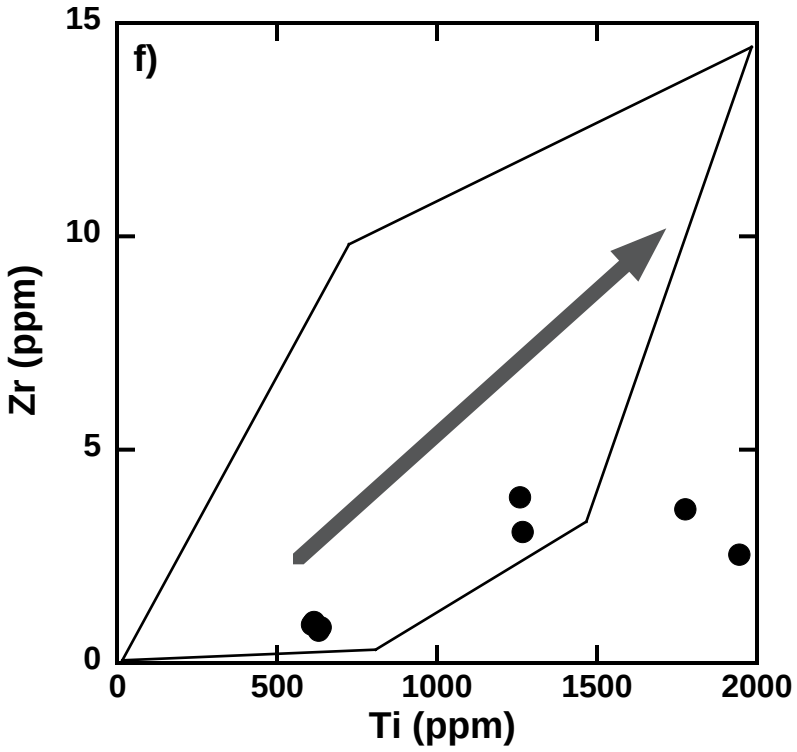

Figure 6f
Wadhwa et al.

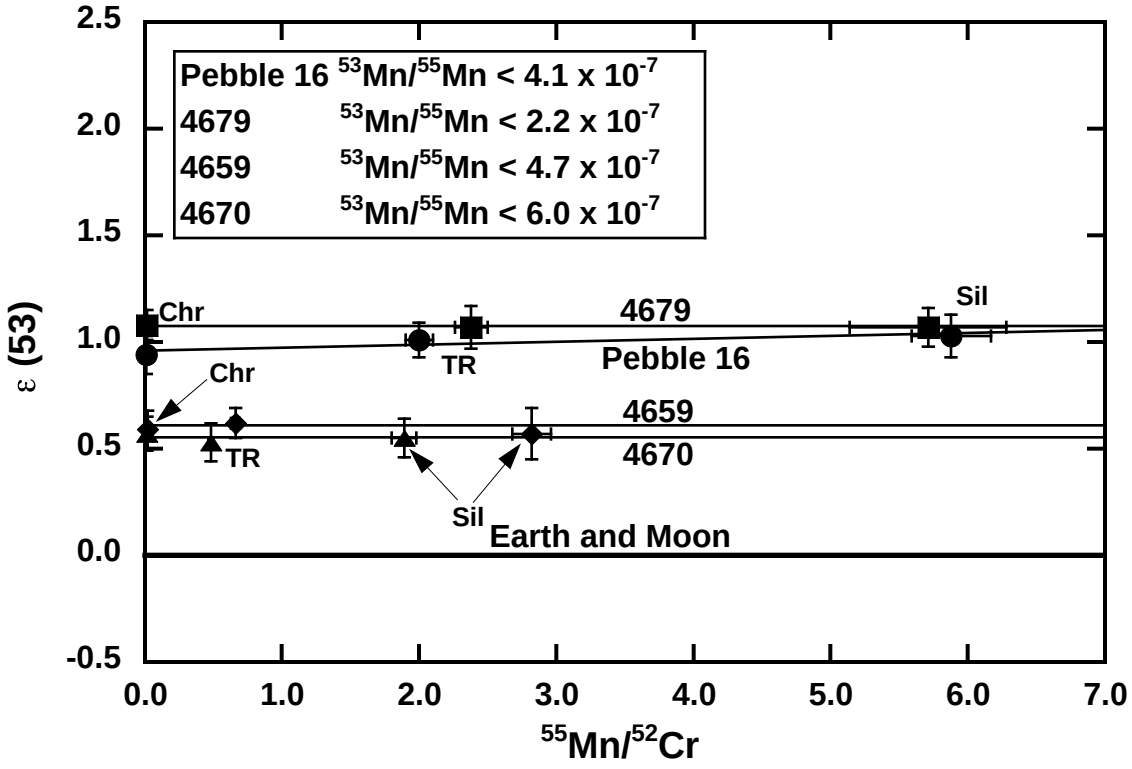

Figure 7
Wadhwa et al.

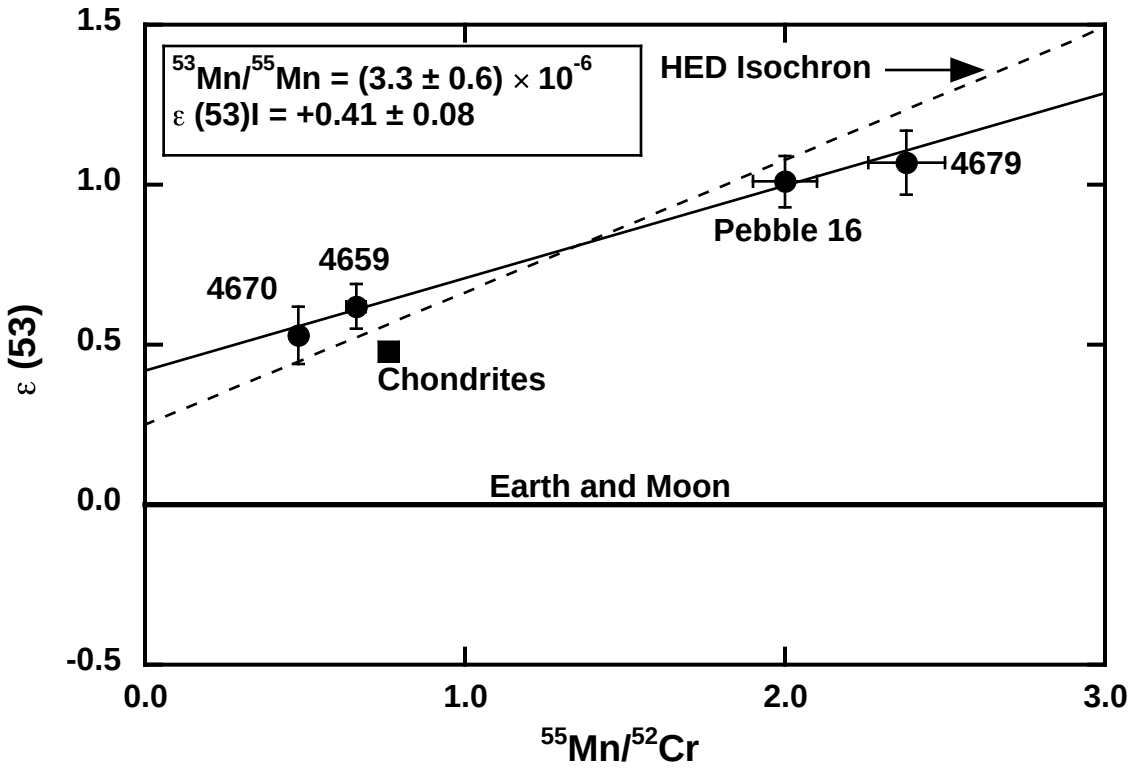

Figure 8
Wadhwa et al.

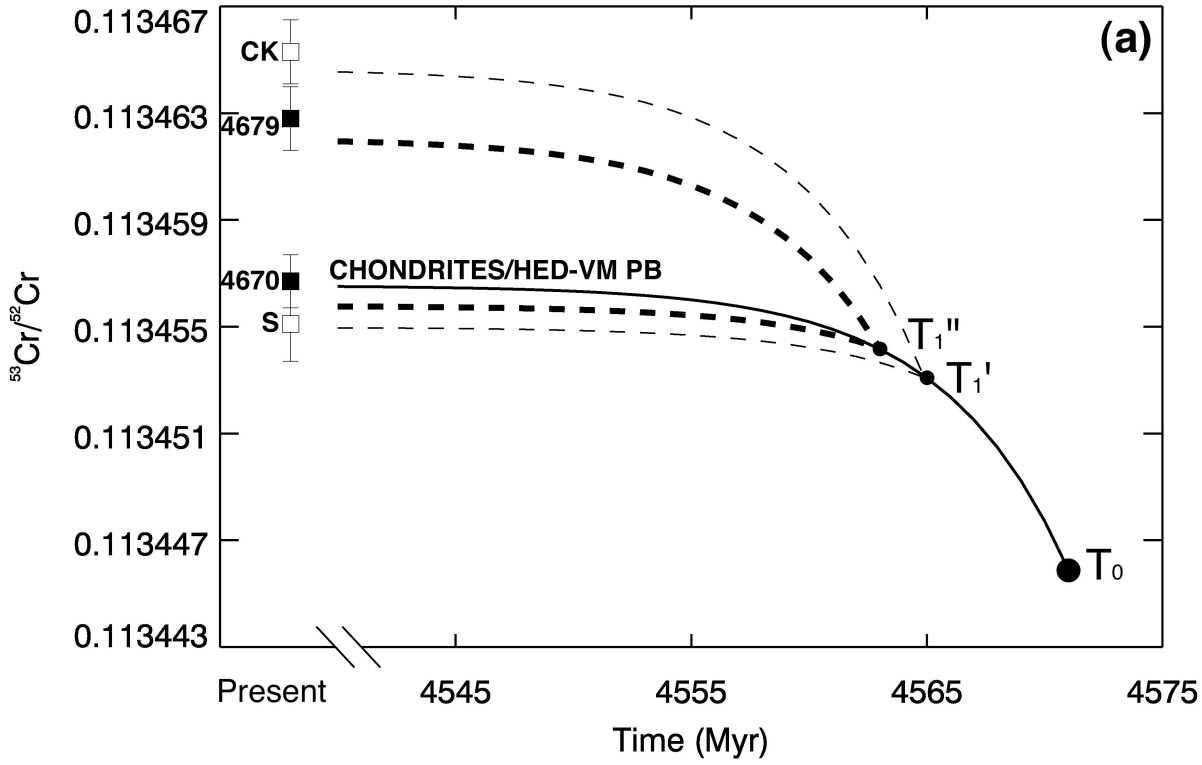

Figure 9a
Wadhwa et al.

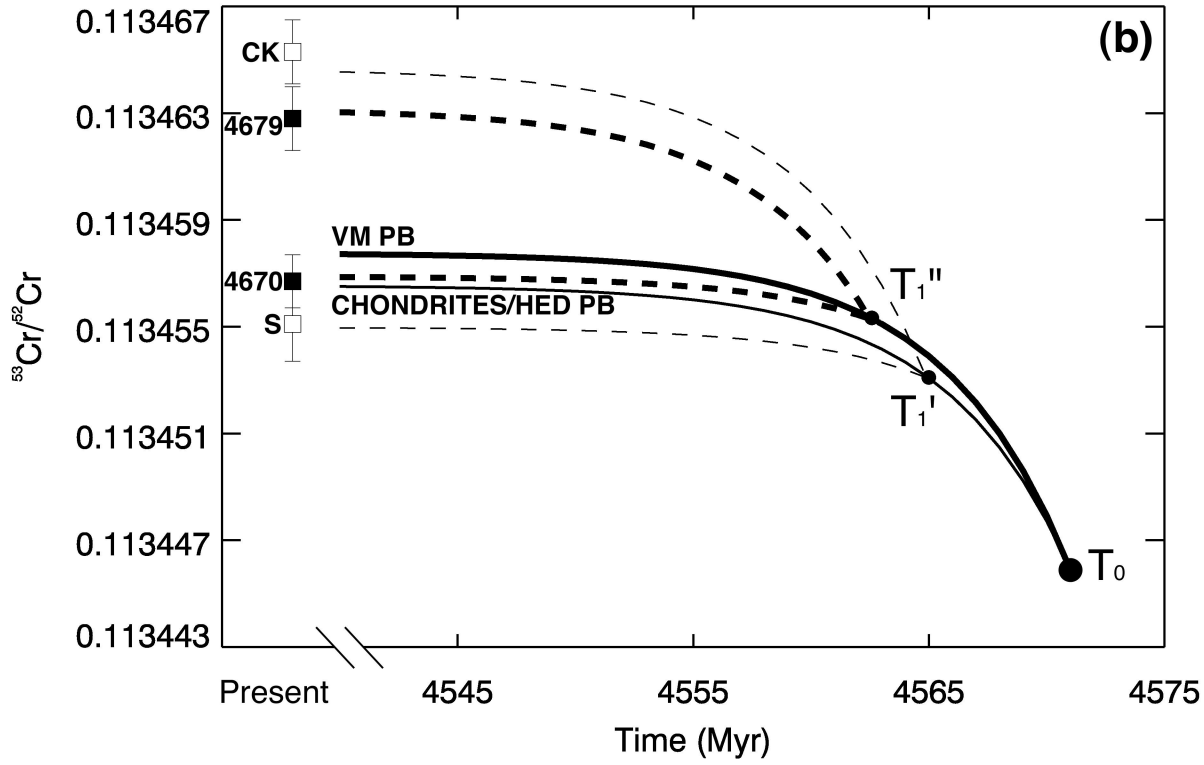

Figure 9b
Wadhwa et al.

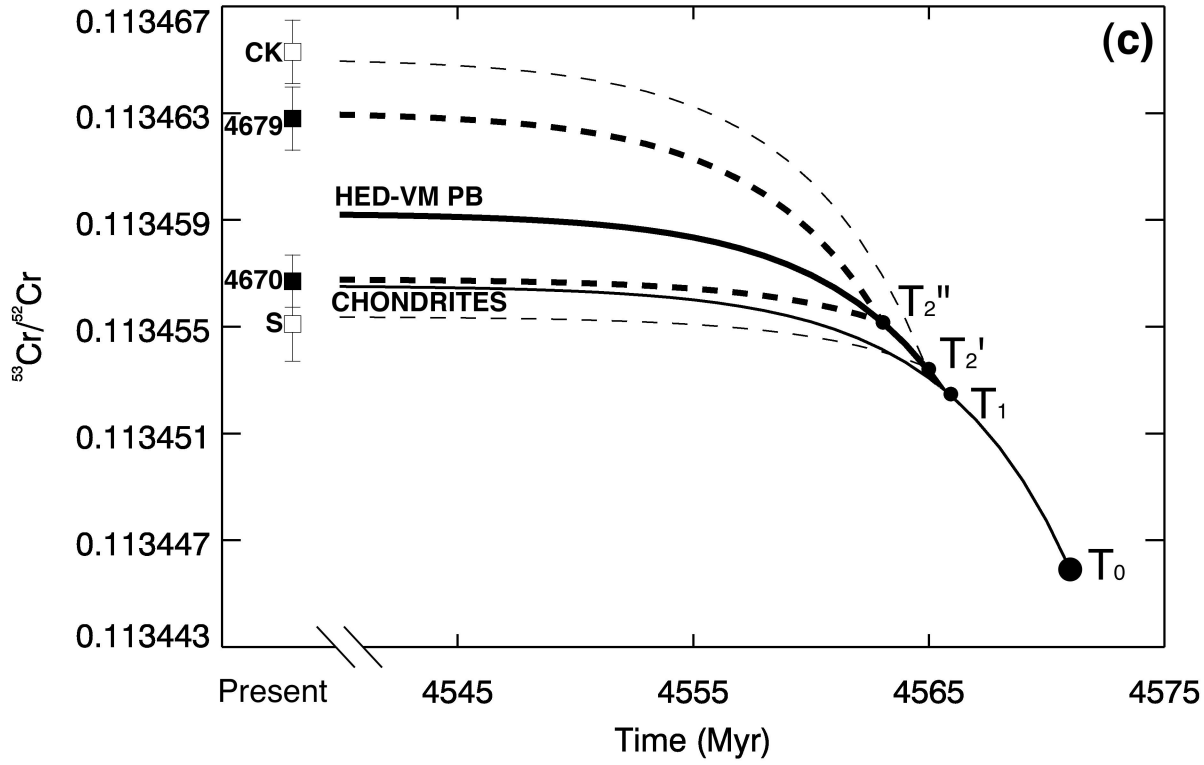

Figure 9c
Wadhwa et al.